bioRχiv

A novel PhoPQ-potentiated mechanism of colistin resistance impairs membrane integrity in *Pseudomonas aeruginosa*

Yu-Ying Phoebe Hsieh[1#*], Ian P. O'Keefe[2,3*], Wanting Sun[1], Zeqi Wang[1], Hyojik Yang[2], Linda M. Vu[2], Robert K. Ernst[2], Ajai A. Dandekar[4,5,], Harmit S. Malik[1,6,**]**

[1]Division of Basic Sciences, Fred Hutchinson Cancer Center, Seattle, Washington, USA; [2]Department of Microbial Pathogenesis, University of Maryland – Baltimore, Maryland, USA; [3]Department of Biochemistry and Molecular Biology, University of Maryland – Baltimore, Maryland, USA; [4]Department of Microbiology, University of Washington, Seattle, Washington, USA; and [5]Department of Medicine, University of Washington, Seattle, Washington, USA; [6]Howard Hughes Medical Institute, Fred Hutchinson Cancer Center, Seattle, Washington, USA

(*These authors contributed equally as co-first authors; **these authors contributed equally)

[#]Correspondence should be addressed to: Yu-Ying Phoebe Hsieh, 1100 Fairview Avenue N. A2-205, Seattle WA 98109; tel: (206) 667-4512; email: yhsieh@fredhutch.org

Keywords: fitness trade-off, lipid A modifications, LPS, experimental evolution, positive epistasis

Polymicrobial communities are often recalcitrant to antibiotic treatment because interactions between different microbes can dramatically alter their responses and susceptibility to antimicrobials. However, the mechanisms of evolving antimicrobial resistance in such polymicrobial environments are poorly understood. We previously reported that Mg^{2+} depletion caused by the fungus *Candida albicans* can enable *Pseudomonas aeruginosa* to acquire significant resistance to colistin, a last-resort antibiotic targeting bacterial membrane. Here, we dissect the genetic and biochemical basis of this increased colistin resistance. We show that *P. aeruginosa* cells can acquire colistin resistance using three distinct evolutionary trajectories involving mutations in genes involved in lipid A biosynthesis, lipid A modifications that are dependent on low Mg^{2+}, and a putative Mg^{2+} transporter, PA4824. These mutations confer colistin resistance by altering acyl chains, hydroxylation, and aminoarabinose modification of lipid A moieties on the bacterial outer membrane. In all cases, enhanced colistin resistance initially depends on the low Mg^{2+}-responsive PhoPQ pathway, which potentiates the evolution of resistance mutations and lipid A modifications that do not occur without Mg^{2+} depletion. However, the PhoPQ pathway is not required to maintain high colistin resistance in all cases. In most cases, the genetic and biochemical changes associated with these novel forms of colistin resistance also impair bacterial membrane integrity, leading to fitness costs. Our findings provide molecular insights into how nutritional competition drives a novel antibiotic resistance mechanism and its ensuing fitness tradeoffs.

Introduction

Antimicrobial resistance poses a global health challenge [1]. Significant research has focused on mechanisms individual bacterial species use to evade antibiotics. However, microbial interactions can profoundly alter antibiotic resistance in ways that are not predictable from the susceptibility of individual species [2, 3]. Complex microbial communities can protect susceptible species from antibiotics and influence the strength of selection, the emergence of resistant mutants, and the identity of resistance mutations. For instance, competitive interactions in polymicrobial biofilms increase mutation rates [4, 5] by inhibiting bacterial growth or inducing radical oxygen species [6]. Similarly, stress response caused by interbacterial competition can increase antimicrobial tolerance [7], facilitating the emergence of resistant mutants [8]. Finally, resource competition can increase the fitness cost of some resistant mutations, limiting their fitness advantage without antibiotics [9]. Despite recent advances in the study of polymicrobial interactions, our knowledge about how microbial interactions drive the evolution of antibiotic resistance remains limited. This is crucial, as polymicrobial infections can exacerbate the spread of drug-resistant bacteria, increasing patient mortality [10, 11] and causing a significant monetary burden on healthcare systems [12]. Further insights into the links between microbial ecology and evolution are critical for developing effective therapies against polymicrobial infections.

Pseudomonas aeruginosa is a gram-negative bacterium frequently found in polymicrobial, drug-resistant nosocomial infections [13, 14]. It commonly coexists with the fungal pathogen *Candida albicans* in urinary tracts, chronic wounds, and the airways of people with cystic fibrosis [15-18]. Polymyxin antibiotics, such as colistin (polymyxin E), are a last resort for treating multi-drug-resistant *P. aeruginosa* infections [19, 20]. Colistin specifically targets gram-negative bacteria by binding to Mg^{2+}-bound lipid A, a hydrophobic domain of lipopolysaccharide (LPS) on the bacterial outer membrane [21, 22], eventually leading to membrane rupture and cell lysis [23].

LPS is the predominant constituent of the outer membrane that protects bacteria from environmental changes [24-26]. Bacteria can rapidly modify lipid A, the membrane-embedded anchor of LPS, to adapt to dynamic environments [27, 28]. Lipid A biosynthesis in gram-negative bacteria begins with the synthesis of lipid IV_A [29], which consists of phosphorylated glucosamine sugars, each serving as the backbone for an N-linked 3'OH-C12 and O-linked 3'OH-C10 acyl chain specifically in *P. aeruginosa* [24, 30, 31]. Subsequently, the HtrB1/LpxO2 and HtrB2/LpxO1 acyltransferases and hydroxylases add secondary O-linked C12 acyl chains [32] and 2' hydroxyl groups [33] at the 3'OH residue of the N-linked acyl chains; such regulation is very conserved in gram-negative bacteria [34-36]. Under normal (Mg^{2+}-replete) conditions, this results in a hexa-acylated, bis-phosphorylated lipid A structure [37, 38]. Mg^{2+}-depletion activates bacterial PhoPQ and PmrAB two-component systems, activating three enzymes that modify lipid A structures [39, 40]. These include PagL [41], a 3'-deacylase that can remove a 3'OH-C10, PagP [42], an acyl transferase that adds a C16, and ArnT [43], which adds 2-amino-2-hydroxy-L-arabinose (aminoarabinose) onto the phosphate decorations to the glucosamine head group. The net effect of these PhoPQ and PmrAB-mediated lipid A modifications is reduced colistin binding to the outer membrane and protection from its antibacterial action [44-46].

In a previous study, we found that *C. albicans* and multiple other fungi can sequester Mg^{2+} from *P. aeruginosa* when grown together in co-culture, thereby inducing Mg^{2+} depletion and leading to colistin resistance in *P. aeruginosa* [47]. Although *P. aeruginosa* could evolve colistin resistance under monoculture (Mg^{2+}-replete) and fungal co-culture (Mg^{2+}-depleted) conditions, we showed that the genetic basis of evolved resistance was distinct in these environments [47]. Monoculture-evolved populations displayed hypermutator phenotypes and acquired mutations in hundreds of genes, including those involved in lipid A modifications. In contrast, co-culture-evolved populations did not increase their mutation rate and acquired mutations only in a few genes, with minimal overlap to the monoculture-acquired adaptive mutations. Moreover, colistin resistance acquired in co-culture remained dependent on *C. albicans* or Mg^{2+} depletion, which was not true for monoculture-acquired colistin resistance [47].

Here, we investigated the biochemical and genetic basis of low Mg^{2+}-dependent colistin resistance in eight replicate *P. aeruginosa* populations that evolved in co-culture with *C. albicans*. Our analyses reveal three distinct, partially overlapping trajectories of colistin resistance, all involving early mutations in genes involved in lipid A biosynthesis, the *oprH*/*phoP*/*phoQ* operon promoter, and *PA4824* – a putative Mg^{2+} transporter. These mutations cause previously unobserved changes in lipid A structure and are sufficient to recapitulate early increases in colistin resistance during evolution. Positive epistasis between these early-evolving mutations and PhoPQ activation largely account for the observed resistance. However, due to a single *htrB2* mutation, bacterial strains in two of three evolutionary trajectories have compromised membrane integrity and significantly reduced fitness in conditions without colistin. Our findings reveal that fungal-bacterial competition for Mg^{2+} can drive novel genetic and biochemical modes of colistin resistance.

Results

P. aeruginosa evolves fungal-dependent colistin resistance via three overlapping but distinct evolutionary trajectories

We previously found that *C. albicans* (and most fungi) could sequester Mg^{2+} from *P. aeruginosa* [47]. To discover whether Mg^{2+} depletion alters the trajectory of colistin resistance, we evolved eight replicate populations of *P. aeruginosa* (wild-type (WT) strain PAO1) through a gradual increase of colistin concentration from 1.5 to 192 μg/ml in co-culture with *C. albicans* in BHI (brain-heart-infusion) media (Fig. 1A). Subsequent analyses revealed that acquired colistin resistance depended on either fungal co-culture or Mg^{2+} depletion. Whole genome sequencing of these eight replicate populations revealed three sets of mutations: lipid A biosynthetic genes, the *oprH*/*phoP*/*phoQ* operon promoter, and *PA4824*, which we previously identified as encoding a novel Mg^{2+} transporter [47] (Fig. 1B).

The first set, comprising replicate populations P2, P3, and P6, showed mutations in *htrB2*, *PA4824*, *oprH*, *fimX*, and *PA3647*. The second set (replicate populations P1, P5, and P7) acquired mutations in *lpxO2*, *htrB2*, and *PA4824*. The third set of replicate populations P4 and P8 had mutations in *lpxA*, *PA4824*, *oprH*, *PA5005*, *pilB*, *colS*, and *ftsY* (Fig. 1B). The only gene mutated in all evolutionary trajectories was *PA4824;* a P224L mutation occurred in seven replicates, and a P224A mutation occurred in one. Replicate populations with shared evolutionary trajectories also exhibited comparable survival when exposed to 192 μg/ml colistin in Mg^{2+}-depleted, fungal co-culture conditions (Fig. S1). Intriguingly, most of the mutations we identified in fungal co-culture-associated colistin resistance were rarely found in monoculture replicate populations subjected to increasing colistin, which instead acquired an almost entirely distinct set of mutations [47]. These findings suggested that increasing colistin challenge elicited three distinct co-culture-specific (or low Mg^{2+}-dependent) colistin resistance trajectories.

We began our studies by investigating the stepwise acquisition of colistin resistance in representatives of the three evolutionary trajectories (replicate populations P2, P5, and P8). We determined the order and timing of mutations by performing whole genome sequencing of evolutionary intermediates, collected and frozen every two weeks, for each replicate population. We found that missense mutations in lipid A biosynthesis genes (*htrB2*, *lpxO2*, and *lpxA*) and the putative Mg^{2+} transporter *PA4824*, as well as mutations in the promoter of the *oprH/phoP/phoQ* operon were fixed relatively early during experimental evolution to increasing colistin dosage (Fig. 1C). For example, *oprH* and *PA4824* (P224L) mutations were fixed by day 21 (6 μg/ml colistin), whereas the *htrB2* (R294H) mutation in replicate P2 was fixed by day 35 (12 μg/ml colistin) (Fig. 1D). In

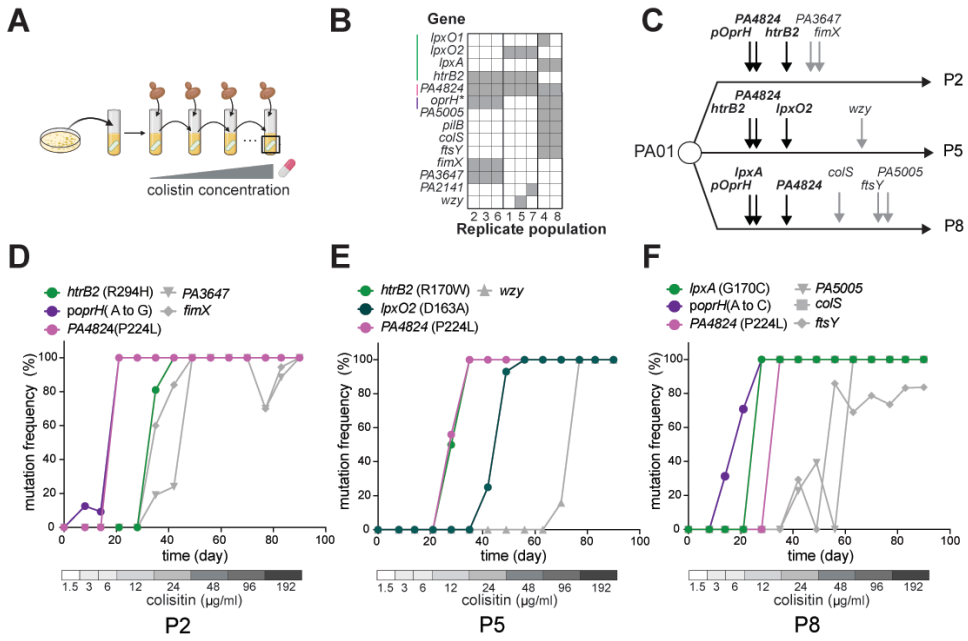

Figure 1. Three distinct evolutionary trajectories lead to fungal-dependent colistin resistance. (A) Schematic of evolving colistin-resistant *P. aeruginosa* in co-culture with *C. albicans*. Eight independent *P. aeruginosa* populations were passaged in BHI with *C. albicans* and colistin. *C. albicans* cells were added at each passage, and the concentration of colistin gradually increased from 1.5 μg/ml to 192 μg/ml. **(B)** Co-culture-evolved populations exhibit three patterns of genetic mutations. Genes mutated in the eight populations are listed in rows, and a mutation in a population is indicated as a gray box. The eight populations are grouped based on the similarity of their mutation patterns. * indicates a mutation in the promoter of the *oprH/phoP/phoQ* operon. **(C)** Summary of the order of mutation fixation in evolved populations P2, P5, and P8. Mutations in lipid A biosynthesis genes, *PA4824*, and the promoter of the *oprH/phoP/phoQ* operon(labeled in black) were fixed in the early stage of evolution across three trajectories. **(D-F)** Temporal dynamics of mutation fixation in evolved populations [P2 (D), P5 (E), P8 (F)]. Mutations in lipid A biosynthesis genes (*htrB2*, *lpxO2*, and *lpxA*), *PA4824*, and the *oprH/phoP/phoQ* promoter became fixed during adaptation to 12-24 μg/ml colistin. The X-axis indicates the day of passage, with the corresponding colistin concentration. The Y-axis represents the frequency of each mutation in the population.

replicate P5, *htrB2* (R170W) and *PA4824* (P224L) mutations were fixed by day 28 (12 μg/ml colistin) with *lpxO2* (D163A) mutation being fixed by day 42 (24 μg/ml colistin) (Fig. 1E). Finally, in replicate P8, the *oprH/phoP/phoQ* promoter mutation arose first and went to fixation together with the *lpxA* (G170C) mutation by day 28 (12 μg/ml colistin), followed by the *PA4824* (P224L) mutation being fixed by day 35 (12 μg/ml colistin) (Fig. 1F). Independent occurrence of mutations in the same gene indicate suggests that these mutations are critical for co-culture-specific colistin resistance.

To further assess their causal role in colistin resistance, we reconstituted single, double, and triple mutations in WT PAO1 to mimic the early stages of bacterial adaptation in the P2, P5, and P8 replicate populations. We then measured colistin's minimum inhibitory concentration (MIC) for each of the reconstructed strains in *C. albicans*-spent BHI (brain-heart-infusion) media, mimicking Mg^{2+} depletion. We found that combinations of early mutations are sufficient to confer significant colistin resistance relative to the WT PAO1 strain (Fig. 2A-C). In all cases, these triple-mutation-reconstructed strains showed resistance to colistin concentrations equivalent to or higher than the colistin concentration used at the time points when these mutations were fixed. Consistent with our MIC estimates, triple-early mutation strains have significantly increased survival at low colistin concentrations from 6 to 24 μg/ml (Fig. S2).

Comparing the colistin resistance of the triple mutant reconstructed strains with either the single or double mutant strains revealed that positive epistasis played a vital role during the evolution of at least two evolutionary trajectories. The most dramatic example of positive epistasis is seen in the P5 population. Single mutants (*oprH*, *PA4824, htrB2)* have no discernible individual effect on colistin resistance, while a double mutant (*htrB2+PA4824*) is modestly resistant (Fig. 2B). However, the triple mutant (*htrB2+PA4824+lpxO2*) is highly resistant (Fig. 2B). The MIC of the P5-derived triple mutant (48 μg/ml) is fourteen-fold higher than the expected MIC from the addition of single mutants, highlighting the role of positive epistasis in the P5 trajectory. In contrast, individual *oprH/phoP/phoQ* promoter mutations were sufficient to confer significant colistin resistance in the P2 and P8 populations, which can be augmented by additional mutations (Fig. 2A, 2C). Intriguingly, although *PA4824* mutations are found recurrently in all eight replicate populations, these mutations did not independently confer any degree of colistin resistance.

Although they account for a measure of colistin resistance, early-occurring triple mutations alone do not confer resistance that can overcome the final colistin concentrations of experimental evolution (192 μg/ml), implying that mutations acquired later in each trajectory are also critical for this additional resistance (Fig. 2A-C). Even though early mutations are insufficient to achieve resistance to 192 μg/ml colistin, they may nevertheless be necessary for high resistance levels. To test this possibility, we reverted each early-occurring mutation in isolates from the endpoint P2, P5, and P8 populations and tested their survival when challenged with 192 μg/ml colistin in Mg^{2+}-depleted conditions. We found that mutation reversion in *htrB2*, *lpxO2*, and the *oprH/phoP/phoQ* promoter significantly reduced bacterial survival. For instance, reverting the *htrB2* mutation to the WT allele in P2 and P5 reduced bacterial survival to ~20% or below (Fig. 2D-E). Similarly, reverting the *oprH/phoP/phoQ* promoter mutation reduced bacterial survival to 20% or 10% in P2 and P8, respectively (Fig. 2D, 2F) while

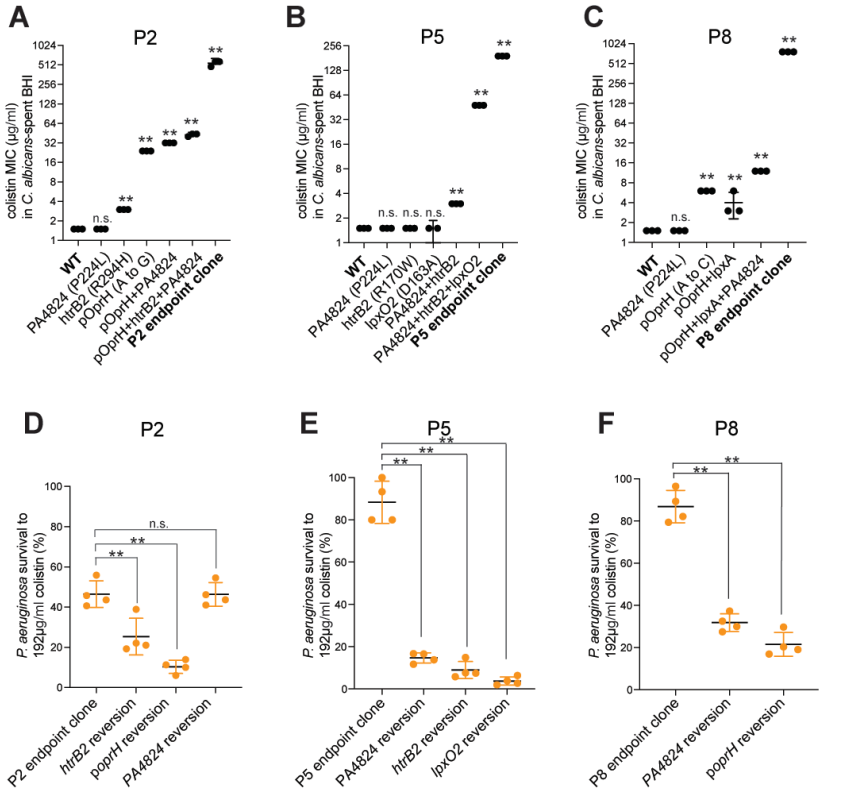

Figure 2. Mutations in lipid A synthetic genes, *PA4824*, and the promoter region of *oprH* are sufficient and necessary for evolving colistin resistance. (A-C) Mutation-reconstructed strains show increased colistin MIC in *C. albicans*-spent media. Colistin MICs of each strain were determined in *C. albicans*-spent media. In three representative populations, MICs of final evolved clones were higher than the final colistin concentration used in the evolution experiment. Panel 2A, 2B, and 2C show results for mutation-reconstructed strains in populations P2, P5, and P8, respectively. Mean ± std of 3 biological replicates is shown (**$p < 0.01$, Dunnett's one-way ANOVA test). **(D-F)** Reversion of mutations in the endpoint clones reduced bacterial survival when treated with 192 ug/ml colistin, in fungal co-culture. **(D)** Reversion of *htrB2* or *oprH*/*phoP*/*phoQ* promoter mutatios to the WT allele in a final P2 clone. **(E)** Reversion of *PA4824*, *htrB2*, or *lpxO2* mutations in a final P5 clone. **(F)** Reversion of *PA4824* or *oprH*/*phoP*/*phoQ* promoter mutation in a final P8 clone. Mean ± std of 4 biological replicates is shown. (**$p < 0.01$, Dunnett's one-way ANOVA test)

reverting the *lpxO2* mutation reduced P5 survival to 3% (Fig. 2E). In contrast, reverting the *PA4824* mutation lowered bacterial survival in P5 and P8, but not P2 (Fig. 2D-F), suggesting that background genetic effects can compensate for *PA4824* evolution in P2. Our findings establish the cadence and causality of the genetic mutations observed in three distinct evolutionary trajectories of Mg^{2+}-depleted colistin resistance. They reveal that "early" mutations in *htrB2*, *lpxO2*, *oprH/phoP/phoQ* promoter, and *PA4824* paved the way for other late-occurring mutations to promote extremely high levels of colistin resistance.

Novel, distinct lipid A structures underlie low Mg^{2+}-dependent colistin resistance in *P. aeruginosa*

Next, we investigated the biochemical basis of acquiring low Mg^{2+}-dependent colistin resistance in our experimentally evolved populations. Previous studies have established that Mg^{2+}-depletion activates the PhoPQ and PmrAB two-component systems, which activate lipid A modifying enzymes, whose action confers resistance to colistin [45, 48]. Our sequencing survey of colistin-resistant populations identified mutations in several genes that affect lipid A structures directly or indirectly (Fig. 1B). For example, the *htrB2* gene involved in lipid A biosynthesis was mutated in two of three evolutionary trajectories, while the *lpxO1*, *lpxO2*, and *lpxA* lipid A biosynthesis genes were mutated in at least one trajectory (Fig. 1B, Fig. 3A). In two of three evolutionary trajectories, we also observed mutations in the *oprH*/*phoP*/*phoQ* operon promoter (Fig. 3A), which might affect PhoPQ-mediated lipid A modification.

To investigate how these lipid A gene mutations lead to colistin resistance, we investigated the biochemical consequences of these mutations on lipid A structure. For this, we used the fast lipid analysis technique (FLAT) and matrix-assisted laser desorption/ionization time-of-flight (MALDI-TOF) mass spectrometry (MS) [49] to determine lipid A structures of all eight endpoint colistin-resistant populations and compared them to WT PAO1. In (Mg^{2+}-replete) BHI media, the WT PAO1 strain exhibited the expected lipid A structures, with penta-acylated lipid A at *m/z* values 1365.89, 1445.86, 1461.85, 1525.82, and 1541.82; all the variation between these ions can be accounted for by altered phosphorylation levels and hydroxylation status (Fig. 3D) [33, 41]. In contrast, all eight replicate populations showed unique mass spectra containing distinctly different lipid A ions compared to WT PAO1. Using principal component analysis (PCA), we analyzed MS data to compare the similarity of lipid A structures from each of the eight replicate populations (Fig. 3C). Our PCA analysis revealed that lipid A structures from the eight evolved populations formed three distinct clusters that can be easily distinguished from WT PAO1, recapitulating the three evolutionary trajectories we had observed previously (Fig. 1B). Our analyses suggest lipid A changes associated with evolved mutations lead to enhanced colistin resistance.

Our FLAT and MALDI-TOF MS analysis identified several novel and previously uncharacterized lipid A structures in the co-culture-evolved replicate populations. We used tandem mass spectrometry (MS/MS) to solve these structures and identify their specific modifications or alterations (Fig. S3). These modifications to lipid A structures include single or double L-Ara4N (aminoarabinose) additions to the phosphate head group decorations, leading to differences of approximately 131 *m/z* in the MS analysis while still maintaining the same acyl chain configuration (Fig. 3E-G, Table S1). Each evolutionary trajectory (PCA cluster) had distinct lipid A structures from WT PAO1 and other reported colistin-resistant strains [50, 51]. For example, populations P2, P3, and P6 exhibited penta-acylated lipid A with PagP-mediated palmitate addition but without HtrB2-mediated laurate addition, leading to *m/z* values of 1501.01, 1632.98, and 1764.03 (Fig. 3E, Table S1). In contrast, populations P1, P5, and P7 exhibited mixtures of two distinct lipid A structures without PagP-mediated palmitate addition.

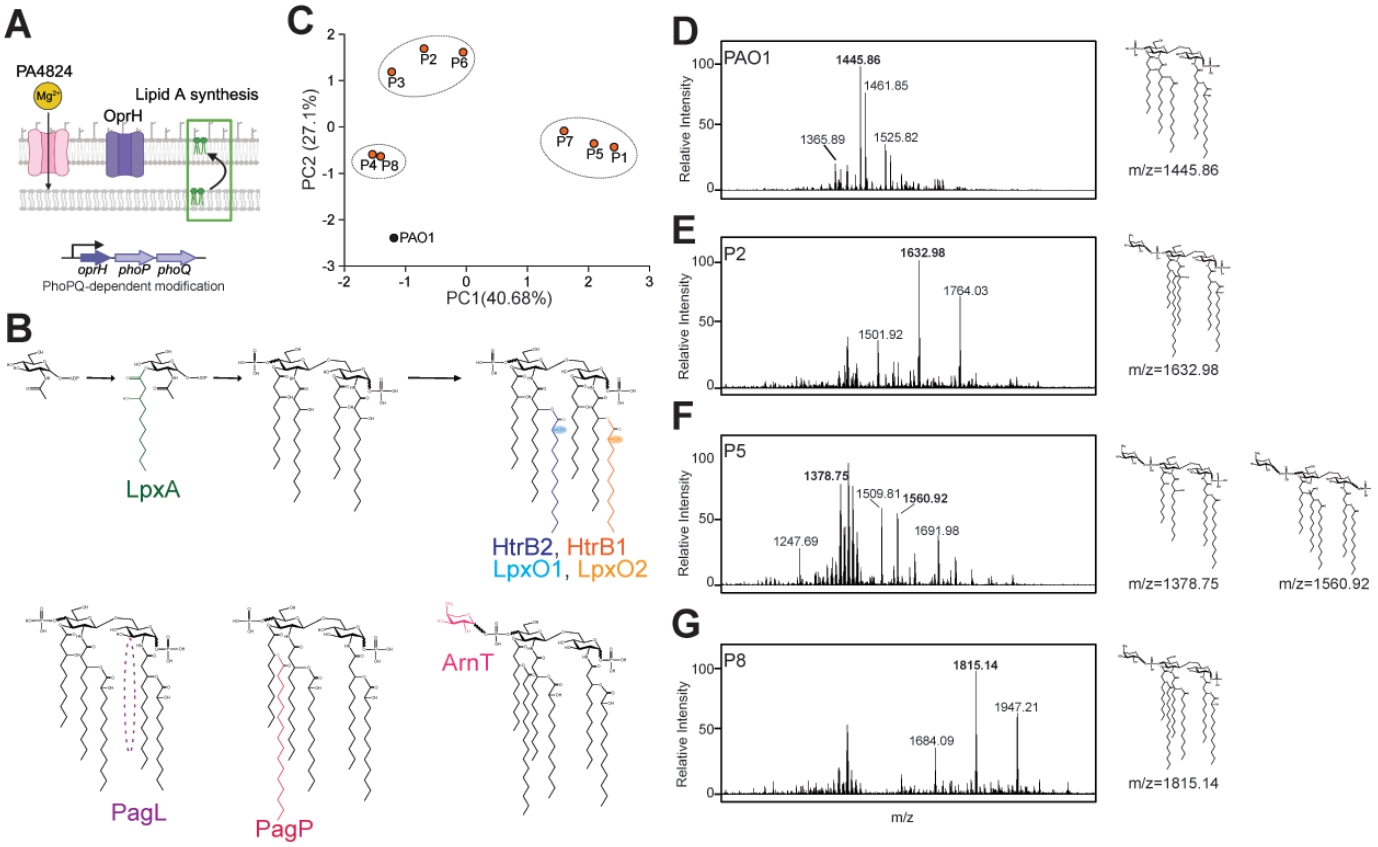

Figure 3. Colistin-resistant populations exhibit novel distinct lipid A structures. (A) Diagram of early evolved mutations. **(B)** Schematic of lipid A biosynthesis pathway and modification. **(C)** Principal Component Analysis (PCA) of lipid A mass spectra from all eight evolved populations and the laboratory-adapted strain PAO1 based on presence or absence of lipid A peaks. PC1 and PC2 are shown, with 40.68% and 27.10% of the variance explained, respectively. Ellipses group strains that cluster together based on observed lipid A structures from FLAT. **(D-G)** Mass spectra of lipid A in PAO1 and evolved populations P2, P5, and P8. **(D)** Lipid A in PAO1 is penta-acylated (m/z = 1445.86) and varies in 2-hydroxylation status (1461.85) and phosphorylation status (1365.89, 1525.82). **(E-G)** Lipid A in all evolved populations exhibits both single and double L-Ara-4-N addition, shown by differences of approximately 131 *m/z*. **(E)** P2 contains lipid A that is penta-acylated, lacking HtrB2-mediated acylation, but contains PagP-mediated C16 addition (*m/z* = 1632.96). **(F)** P5 contains lipid A lacking HtrB2-mediated acylation and LpxO2-mediated 2-hydroxylation (*m/z* = 1378.75). P5 also shows the presence of lipid A containing HtrB2-mediated acylation but lacking both LpxO1 and LpxO2-mediated 2-hydroxylation (*m/z* = 1560.92). **(G)** P8 contains hexa-acylated lipid A with PagP-mediated palmitoylation (*m/z* = 1815.14).

These include tetra-acylated lipid A, lacking both HtrB2-mediated acylation and LpxO2-mediated hydroxylation (*m/z* = 1247.69, 1378.75, 1509.81), as well as penta-acylated lipid A, containing HtrB2-mediated laurate addition but lacking both LpxO1 and LpxO2-mediated hydroxylation (*m/z* = 1560.92, 1691.98) (Fig. 3F, Table S1). Finally, populations P4 and P8 exhibited hexa-acylated lipid A containing PagP-mediated palmitate addition but lacking LpxO1-mediated hydroxylation (*m/z* = 1684.09, 1815.14, 1947.21) (Fig. 3G, Table S1).

To determine if these changes were triggered by fungi or Mg^{2+} depletion – the condition in which our experimental evolution occurred – we compared our lipid A structures between *P. aeruginosa* populations grown in the presence or absence of *C. albicans* in BHI media. We found no significant changes between these two conditions (Fig. S3). Thus, biochemical changes in lipid A structures are not dependent on induced physiological responses to the presence of *C. albicans* or Mg^{2+} depletion. Instead, these changes are genetically determined by adaptive mutations selected during experimental evolution.

To identify which mutations led to the unique lipid A structures we observed, we analyzed the lipid A structures of early-occurring triple mutant reconstructed strains from all three evolutionary trajectories (P2, P5, and P8) using FLAT followed by MALDI-TOF MS. In all three trajectories, additions of aminoarabinose to lipid A were observed in mutation-reconstructed strains (Fig. S4). We found that early-occurring mutations in just three genes can recapitulate the distinctive changes in lipid A in two of three evolutionary trajectories (P2, P5), with partial recapitulation for the third (P8) (Fig. S4). For instance, the triple mutant strain with *PA4824*, *htrB2*, and *oprH/phoP/phoQ* promoter mutations exhibited the same ions as the P2 endpoint strain. Similarly, the triple mutant strain containing *PA4824*, *htrB2*, and *lpxO2* mutations recapitulated the lipid A changes of the P5 endpoint strain. For the P8 trajectory, the early-occurring triple mutant strain with *PA4824*, *oprH/phoP/phoQ* promoter, and *lpxA* mutations also yielded most of the hexa-acylated lipid A structure containing PagP-mediated palmitoylation as the P8 endpoint strain. However, we also observed additional ions at *m/z* = 1445.86 and 1576.91 in the early-occurring triple mutants in the P8 trajectory that were absent in P8 endpoint strains. Additional ions were present approximately 16 m/z above previously reported ions, indicating the presence of LpxO1-mediated hydroxylation. These indicate the additional presence of lipid A without PagP-mediated palmitoylation and double lipid A 2- hydroxylation. Thus,

the trio of early mutations in P8 cannot completely mimic the phenotypic loss-of-function of LpxO1 or constitutive PagP activation that occurred in the later stages of the P8 evolutionary trajectory.

We also analyzed the effect of single mutation reversion on lipid A structures of the P2, P5, and P8 endpoint strains. We found that reverting *htrB2* or *oprH/phoP/phoQ* promoter mutations restored function and partially restored lipid A structures to resemble WT, whereas reversion of the *PA4824* mutations had no impact on lipid A structures (Fig. S5). Overall, our mutation reconstruction and reversion experiments reveal that loss-of-function mutations in *htrB2* and *lpxO2* cooperate with the *oprH*/*phoP*/*phoQ* promoter mutations to alter lipid A structures and increase colistin resistance during evolution, potentially by decreasing colistin binding to bacterial outer membranes. Despite the importance of *htrB2* and *lpxO2* in the lipid A biosynthesis in *P. aeruginosa* [32, 52], our findings suggest that mutations in both genes significantly confer colistin resistance in Mg^{2+} depleted conditions.

PhoPQ synergizes with early-occurring mutations to potentiate colistin resistance

In two of three evolutionary trajectories, mutations upstream of the *oprH*/*phoP*/*phoQ* operon arose first in the P2 and P8 populations. This finding suggests that activation of the PhoPQ pathway is required to evolve increased resistance under Mg^{2+} depletion in these populations. To test this possibility, we first examined whether introducing the two distinct *oprH*/*phoP*/*phoQ* promoter mutations in WT PAO1 led to any distinctive changes in their lipid modifications. Indeed, we found that single promoter mutations recapitulate the same L-Ara4N modification and PagP-mediated acylation observed in populations P2 and P8 (Fig. 4A and 4B), suggesting that they are sufficient to activate PhoPQ-mediated lipid A modifications. In a second confirmation, we deleted either *oprH* or *phoP*, the transcriptional regulator of the PhoPQ pathway, in endpoint isolates from populations P2 and P8. In both, the deletion of *phoP* significantly decreased colistin MIC in Mg^{2+}-depleted media and completely abrogated L-Ara4N modification and PagP-mediated acylation, consistent with previous reports [44, 48] (Fig. S6). In contrast, Δ*oprH* mutants had either a modest or no effect on colistin resistance in the P2 and P8 endpoint clones (Fig. S7). Based on these findings, we conclude that the *oprH*/*phoP*/phoQ promoter mutations were selected for their effect on the PhoPQ pathway and not on *oprH*.

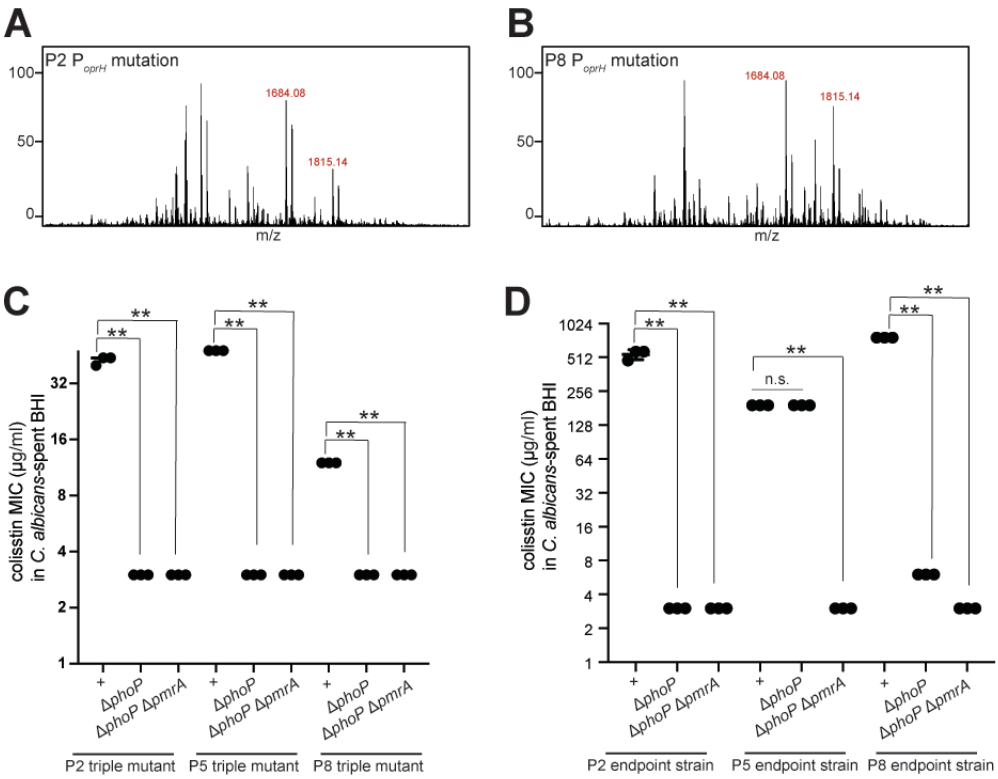

Figure 4. PhoPQ pathway acts synergistically with early-occurring mutations to confer colistin resistance. (A-B) Mass spectra of lipid A in PAO1 containing the mutation in the *oprH/phoP/phoQ* operon from P2 (A) and P8 (B). The *m/z* peak representing PhoPQ activity is labeled in red: 1684.08 represents lipid A with PagP-mediated acylation but without L-Ara4N addition. 1815.14 represents lipid A with PagP-mediated acylation and L-Ara4N addition. **(C)** Colistin resistance in the early genetic backgrounds of P2, P5, and P8 require PhoPQ activity. Δ*phoP* or Δ*phoP* Δ*pmrA* in triple mutants of three evolutionary trajectories are shown. Colistin resistance was measured by the standard MIC assay in Mg^{2+}-depleted *C. albicans*-spent media. Mean ± std of 3 biological replicates is shown. (**$p < 0.01$, Dunnett's one-way ANOVA test). **(D)** Colistin resistance in the endpoint clone of P2 and P8, but not P5, require PhoPQ activity. Δ*phoP* or Δ*phoP* Δ*pmrA* in the endpoint clones of three evolutionary lineages are shown. Colistin resistance was measured by the standard MIC assay in Mg^{2+}-depleted *C. albicans*-spent media. Mean ± std of 3 biological replicates is shown. (**$p < 0.01$, Dunnett's one-way ANOVA test)

Mg^{2+} depletion activates both the PhoPQ and the PmrAB pathways [39, 40]. To further assess the role of PhoPQ in conferring resistance, we investigated whether *phoP* deletion in the early-occurring triple mutants of P2, P5, or P8 also significantly reduced colistin resistance. Indeed, this was the case; colistin MIC was reduced to 3 µg/ml (Fig. 4C) in the early stages of all three evolutionary trajectories upon *phoP* deletion. Furthermore, colistin resistance was not further reduced upon additional loss of *pmrA* (Fig. 4C). Based on these findings, we conclude that PhoPQ dominantly potentiates colistin resistance in all three of the Mg^{2+}-depleted evolutionary trajectories by synergizing with other early-occurring mutations.

Finally, we tested whether the colistin resistance of the final endpoint clones continued to depend on PhoPQ (Fig. 4D). To our surprise, we found this was only sometimes the case. Whereas PhoPQ continued to be required for the high colistin resistance of the P2 and P8 endpoint clones, it was unexpectedly dispensable for the P5 endpoint clone, which became more dependent on the PmrAB pathway. Since the final endpoint P5 clone only has one additional mutation in the *wzy* gene, a polymerase for O-antigen of LPS [53, 54] (Fig. 1), this mutation must be necessary and sufficient to both enhance colistin resistance of the P5 clone and switch its dependence from the PhoPQ to the PmrAB pathway.

Colistin resistance evolved under Mg^{2+} depletion compromises membrane integrity

We investigated the biological outcomes of the distinctive lipid A structures in our experimentally evolved colistin-resistant populations on phenotypes beyond colistin resistance. First, we performed scanning electron microscopy (SEM) in Mg^{2+}-replete BHI media to investigate whether structural changes in lipid A result in visible abnormalities in cell morphology. We found differences in cell morphology between all three evolved evolutionary trajectories. The P2 endpoint clone had the most severe cell morphological defects, showing shorter cells and dramatic membrane kinks. P5 cells were modestly altered, with elongations and membrane kinks. On average, P8 cells did not exhibit any apparent membrane kinks in the SEM analyses

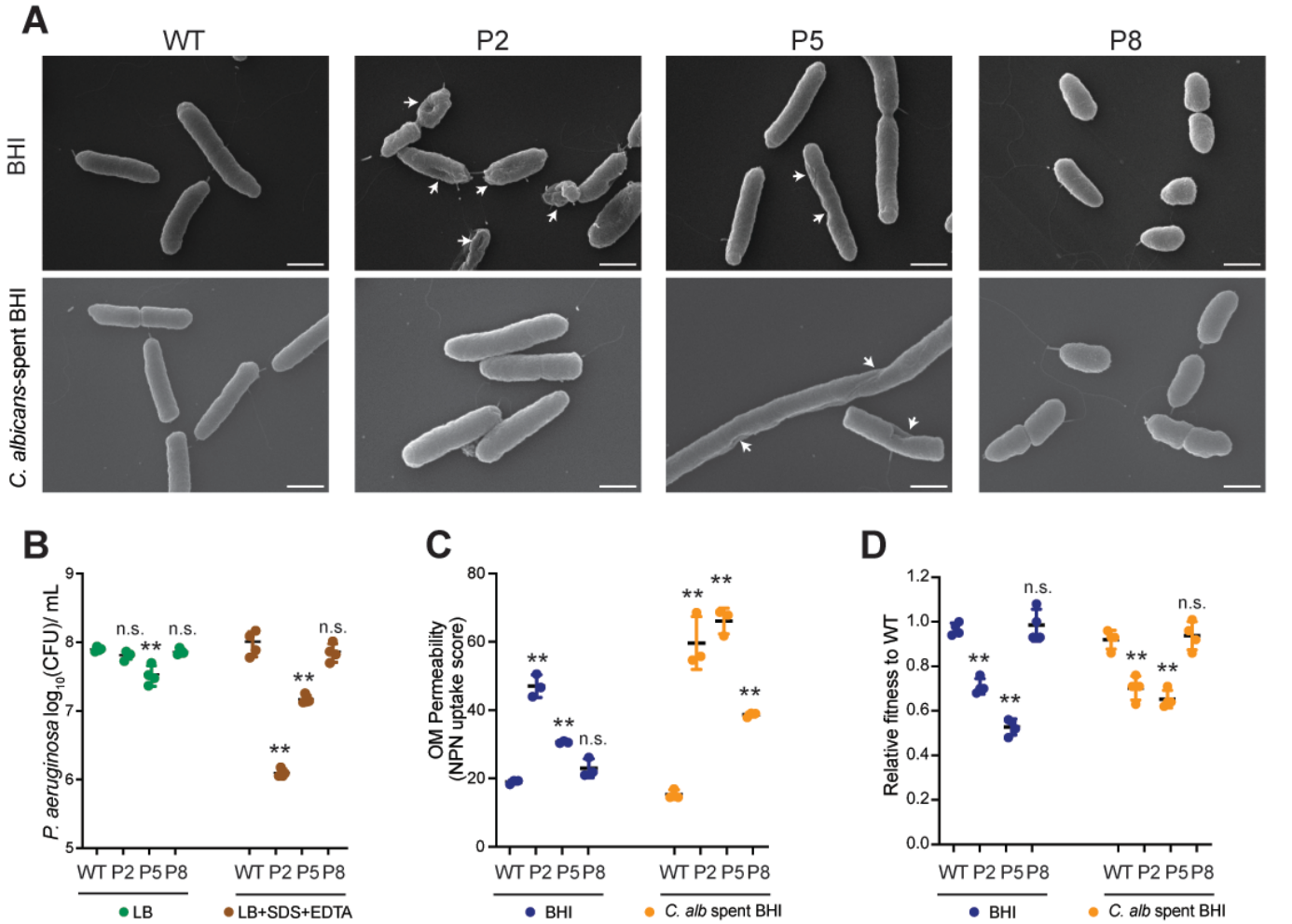

Figure 5. Colistin-resistant populations have fitness costs due to defective membrane integrity. (A) Scanning electron microscopic images of P2, P5, and P8 endpoint strains in (Mg^{2+}-replete) BHI and (Mg^{2+}-depleted) *C. albicans*-spent BHI. In BHI, P2 and P5, but not P8, had dents or kinks in the cell membrane (white arrows). In *C. albicans*-spent BHI, only P5 showed membrane deformation. All three displayed altered cell shapes compared to WT PAO1. Scale bar indicates 1μm. **(B)** P2 and P5, but not P8, are more sensitive to membrane stress. Log-phase cells were grown in monoculture and serially diluted on LB plate (green) or LB plate supplemented with SDS and EDTA (brown) to assay bacterial resistance to membrane-perturbing agents. Mean ± std of 4 biological replicates is shown. (**$p < 0.01$, Dunnett's one-way ANOVA test)**. (C)** All three lineages have increased outer membrane permeability in Mg^{2+}-depleted media. An NpN assay was used to measure outer membrane permeability of WT and three the representative evolved populations P2, P5, and P8. Mean ± std of 3 biological replicates is shown. (**$p < 0.01$, Dunnett's one-way ANOVA test). **(D)** Endpoint strains of P2 and P5, but not P8, show reduced fitness in monoculture and co-culture without colistin. A competitive fitness assay was used to measure the relative fitness of three representative evolved populations, P2, P5, and P8, to WT PAO1. Mean ± std of 3 biological replicates is shown. (**$p < 0.01$, Dunnett's one-way ANOVA test)

but were shorter than WT cells (Fig. 5A). Intriguingly, many of these evident membrane defects appear to be rescued in fungal-spent Mg^{2+}-depleted BHI media. The most dramatic example of this is seen in cells from the P2 lineage, whose significant defects in morphology in BHI media were largely rescued in Mg^{2+}-depleted BHI media (Fig. 5A).

Next, we asked whether the observed changes in lipid A modifications and cell morphological aberrations alter the membrane integrity of the final evolved clones from each of the three evolutionary trajectories. First, we assessed the growth of evolved strains in normal conditions (LB media) or membrane-perturbing conditions, such as LB media with SDS and EDTA [55]. We found no dramatic differences in growth between WT and either P2 or P8 endpoint clones in LB media, but P5 cells were growth-impaired even in LB media alone (Fig. 5B). Moreover, evolved clones from P2 and P5 displayed higher sensitivity to membrane-perturbing agents (LB+SDS+EDTA) than WT cells, whereas P8 cells were relatively unimpaired (Fig. 5B).

In a second assay, we used uptake of a fluorometric NPN (1-N-phenylnaphthylamine) to measure outer membrane permeability [23]. We found that P2 and P5 exhibited higher NPN uptake in Mg^{2+}-replete BHI media; although P8 cells also had higher NPN uptake than WT cells in BHI media, this difference was not significant (Fig. 4C). However, in Mg^{2+}-depleted *C. albicans*-spent BHI media, we found that all three experimentally evolved endpoint clones – P2, P5, P8 – had higher NPN uptake scores than WT. This suggests that all three evolutionary trajectories for higher colistin resistance lead to severe membrane integrity defects, further exacerbated upon Mg^{2+} depletion (Fig. 5C), even though Mg^{2+} depletion rescued some of the morphological defects seen in these lineages (Fig. 5A).

Finally, we investigated whether loss of membrane integrity affects bacterial fitness in the absence of colistin. Indeed, we found that the fitness of P2 and P5 was 40% lower than WT in both monoculture and co-culture conditions when colistin was absent (Fig. 4D). These fitness defects manifest even in the early-evolved triple mutant P2 and P5 strains (Fig. S8), suggesting that increased colistin resistance is coupled with compromised bacterial membrane integrity relatively early in the experimental evolution of the P2 and P5 evolutionary trajectories. This trend is correlated with the degree of membrane defects of these three populations, suggesting different evolutionary lineages lead to different fitness costs despite many shared overlapped mutations.

The lower fitness of P2 and P5, but not P8, endpoint strains led us to hypothesize that the loss-of-function *htrB2* mutations (found in P2 and P5 but not P8) are primarily responsible for the fitness cost and higher membrane integrity defects seen in P2 and P5 trajectories. We tested this hypothesis by reverting *htrB2* mutation to WT in P2 and P5 endpoint strains. We found that the *htrB2* reversion was sufficient to significantly increase bacteria fitness in co-culture and monoculture conditions (Fig. S9). Thus, we conclude that *htrB2* loss-of-function mutations in two independent evolutionary trajectories cause fitness loss, potentially by compromising bacterial membranes. This lower fitness could explain why we do not observe P2 or P5-like trajectories upon experimental evolution for colistin resistance in (Mg^{2+}-replete) monoculture conditions. Indeed, an Δ*htrB2* mutant in WT PAO1 decreases colistin resistance in Mg^{2+}-replete conditions [32], further emphasizing the effects of nutritional competition on the genetic trajectories of acquiring colistin resistance.

Unlike P2 and P5 endpoint clones, the P8 endpoint clones do not appear to be fitness-impaired relative to WT cells. However, closer examination of the early-occurring triple mutant P8 strain reveals that even this lineage is initially impaired for fitness relative to WT cells without colistin (Fig. S8). Thus, later-occurring mutations in the P8 trajectory have partially restored the early fitness costs of the P8 trajectory. Nevertheless, the early impairment of fitness may have been sufficient to prevent the P8-like trajectory from occurring under (Mg^{2+}-replete) monoculture conditions.

Discussion

The evolution of microbial traits, such as antibiotic resistance, is driven by the environments microbe live in and their interactions with co-inhabiting species [56-58]. However, there is little experimental evidence to dissect how interspecies interactions affect the evolution of antibiotic resistance. In this study, we investigated the molecular and biochemical bases by which Mg^{2+} sequestration by *C. albicans* alters the acquisition of colistin resistance in *P. aeruginosa* [47]. We found that the PhoPQ pathway activated by low Mg^{2+} enables the bacteria to evolve resistance through three distinct evolutionary trajectories involving a distinctive set of mutations targeting genes involved in lipid A biosynthesis, modification, and PA4824; these mutations do not occur in Mg^{2+}-replete conditions. We show that combining just three early-occurring mutations in each trajectory is sufficient and necessary for enhanced colistin resistance by significantly altering lipid A structures with changes in acyl chains and hydroxylation. Although this adaptation mode is effective, such lipid A alteration makes the bacterial outer membrane leakier, leading to strong morphological and fitness defects in the absence of colistin. Overall, our work reveals how nutritional competition for Mg^{2+} between fungi and gram-negative bacteria such as *P. aeruginosa* unexpectedly potentiates novel molecular mechanisms of colistin resistance with unique fitness tradeoffs.

The colistin-resistant evolved bacteria present a new molecular mode of colistin resistance. *P. aeruginosa* is known to acquire colistin resistance by adding L-Ara4N to the lipid A moiety of LPS, mediated by the *PA3552-PA3559* operon [44]. Mutations in genes regulating this operon, such as *pmrAB* and *phoPQ*, commonly occur in clinical *P. aeruginosa* isolates [59, 60] and experimentally evolved strains [61, 62]. And yet, we provide molecular evidence that loss-of-function mutations in *htrB2* and *lpxO2*, which alter acyl chains and hydroxylation of lipid A, are necessary for evolving increased colistin resistance in Mg^{2+}-depleted conditions. However, their individual effects on colistin resistance depend on the genetic background. Individual *htrB2* or *lpxO2* mutations do not confer resistance unless combined with mutations in the *oprH/phoP/phoQ* promoter and *PA4824*, highlighting the role of positive epistasis. Intriguingly, *lpxO2* loss-of-function mutations have been previously observed in several cystic fibrosis-associated *P. aeruginosa* isolates but are not directly implicated in colistin resistance

[33, 63]; we speculate that these mutations might enhance colistin resistance in environments where bacteria co-occur with fungi.

Despite the genes involved in lipid A biosynthesis being well-characterized, our findings suggest that the roles of mutations in this pathway and their interactions with other mutations remain an exciting discovery area. For example, MS analysis revealed several unexpected changes in lipid A structures that genetic mutations in lipid A-modifying genes cannot fully explain. For instance, despite having a WT copy of *lpxO1*, population P8 lacked LpxO1-mediated hydroxylation. Similarly, despite not having *lpxO1* mutation in P5, some lipid A spectra represent the lack of LpxO1-mediated hydroxylation activity. Finally, population P5, carrying a *htrB2* mutation (R170W), exhibited a heterogenous presence of HtrB2-mediated acylation in the lipid A mass spectra. These findings indicate that other evolved mutations in these two populations may rewire the genetic requirements for lipid A structures, suggesting the involvement of unidentified pathways in HtrB2 and LpxO1-mediated activities.

One gene that contributes to colistin resistance in Mg^{2+}-depleted conditions through still unknown mechanisms is *PA4824* – the only gene recurrently mutated by missense mutations in the same residue (P224) in all eight replicate populations we studied. We previously showed that *PA4824* might act as an Mg^{2+} transporter, like *mgtA* [47]. In two of three evolutionary trajectories, *PA4824* mutations interact with mutations in lipid A-related genes to confer resistance. However, we found no evidence that *PA4824* plays a direct role in lipid A modifications. Moreover, the loss of the *PA4824* mutations affects colistin resistance only in a subset of endpoint clones. Future studies might explore how the *PA4824* mutation, alone or in combination with other mutations, might alter the biophysical property of the outer bacterial membrane to enhance colistin resistance.

Our findings also reveal a more complex role for PhoPQ in colistin resistance upon Mg^{2+} depletion than previously appreciated. It has long been known that Mg^{2+} depletion induces PhoPQ pathway activation, which results in lipid A modifications that lower colistin binding to outer bacterial membranes [40, 48]. Our findings reveal that, upon chronic fungal-mediated Mg^{2+} depletion, PhoPQ synergizes with unique adaptive mutations – many (such as *htrB2*) that would never occur under Mg^{2+} replete conditions – to catalyze unique lipid A-altering mutations crucial for early colistin resistance in low Mg^{2+} conditions. Surprisingly, although PhoPQ potentiates early colistin resistance in all three evolutionary trajectories, it is not required to maintain high colistin resistance in all trajectories. The P5 trajectory has switched from PhoPQ to PmrAB dependence between early and endpoint stages, likely mediated by mutations in the *wzy* gene, which provides novel insights into the rewiring of stress response pathways in bacteria.

Our findings reinforce previous findings that nutritional competition for Mg^{2+} plays a critical role beyond simply being a trigger for the PhoPQ pathway and resistance to colistin. For example, magnesium depletion can affect the expression of genes not directly controlled by PhoPQ, such as *retS*, leading to increased aggregate or biofilm formation [64] that could prevent colistin binding to bacteria. Similarly, Mg^{2+} depletion can directly mediate L-Ara4N modifications to lipid A in a PmrAB-dependent but PhoPQ-independent manner [65-67]. Finally, Mg^{2+} depletion could affect cellular energetics and membrane potential [68], impacting bacterial metabolism and response to colistin.

Our study highlights the adaptability of *P. aeruginosa* to colistin upon Mg^{2+} depletion (fungal-mediated or otherwise), primarily through alterations in lipid A. Lipid A is a critical component of the bacterial membrane that plays a crucial role in bacterial survival under various environmental stresses [27]. Future studies could explore the broader biomedical consequences of the lipid A changes identified in our experiments, such as their potential impact on host immune evasion or cross-resistance to other antibiotics in *P. aeruginosa*. Additionally, our molecular and biochemical findings provide a foundation to investigate whether similar lipid A alterations occur in clinical or environmental isolates of *P. aeruginosa* and other gram-negative bacteria of high biomedical interest.

References

1. Huemer, M., et al., *Antibiotic resistance and persistence-Implications for human health and treatment perspectives.* Embo Reports, 2020. **21**(12).
2. Bottery, M.J., J.W. Pitchford, and V.P. Friman, *Ecology and evolution of antimicrobial resistance in bacterial communities.* Isme Journal, 2021. **15**(4): p. 939-948.
3. De Wit, G., et al., *Microbial Interspecies Interactions and Their Impact on the Emergence and Spread of Antimicrobial Resistance.* Annual Review of Microbiology, 2022. **76**: p. 179-192.
4. Frapwell, C.J., et al., *Increased rates of genomic mutation in a biofilm co-culture model of Pseudomonas aeruginosa and Staphylococcus aureus.* 2018.
5. Trejo-Hernández, A., et al., *Interspecies competition triggers virulence and mutability in Candida albicans-Pseudomonas aeruginosa mixed biofilms.* Isme Journal, 2014. **8**(10): p. 1974-1988.
6. Maharjan, R.P. and T. Ferenci, *The impact of growth rate and environmental factors on mutation rates and spectra in Escherichia coli.* Environ Microbiol Rep, 2018. **10**(6): p. 626-633.
7. Lories, B., et al., *Biofilm Bacteria Use Stress Responses to Detect and Respond to Competitors.* Curr Biol, 2020. **30**(7): p. 1231-1244 e4.
8. Levin-Reisman, I., et al., *Antibiotic tolerance facilitates the evolution of resistance.* Science, 2017. **355**(6327): p. 826-830.
9. Klümper, U., et al., *Selection for antimicrobial resistance is reduced when embedded in a natural microbial community.* Isme Journal, 2019. **13**(12): p. 2927-2937.
10. Ferreiro, J.L.L., et al., *Pseudomonas aeruginosa urinary tract infections in hospitalized patients: Mortality and prognostic factors.* Plos One, 2017. **12**(5).
11. Lechtzin, N., et al., *Outcomes of adults with cystic fibrosis infected with antibiotic-resistant Pseudomonas aeruginosa.* Respiration, 2006. **73**(1): p. 27-33.
12. Group, I.P.C., *Global burden associated with 85 pathogens in 2019: a systematic analysis for the Global Burden of Disease Study 2019.* Lancet Infect Dis, 2024. **24**(8): p. 868-895.

13. Pang, Z., et al., *Antibiotic resistance in Pseudomonas aeruginosa: mechanisms and alternative therapeutic strategies.* Biotechnology Advances, 2019. **37**(1): p. 177-192.
14. Cao, P., et al., *A Pseudomonas aeruginosa small RNA regulates chronic and acute infection.* Nature, 2023. **618**(7964): p. 358-364.
15. Bauernfeind, A., et al., *Qualitative and quantitative microbiological analysis of sputa of 102 patients with cystic fibrosis.* Infection, 1987. **15**(4): p. 270-7.
16. Kahl, L.J., et al., *Interkingdom interactions between Pseudomonas aeruginosa and Candida albicans affect clinical outcomes and antimicrobial responses.* Current Opinion in Microbiology, 2023. **75**.
17. Timm, M.R., S.K. Russell, and S.J. Hultgren, *Urinary tract infections: pathogenesis, host susceptibility and emerging therapeutics.* Nat Rev Microbiol, 2024.
18. Malhotra, S., D. Hayes, Jr., and D.J. Wozniak, *Cystic Fibrosis and Pseudomonas aeruginosa: the Host-Microbe Interface.* Clin Microbiol Rev, 2019. **32**(3).
19. Ledger, E.V.K., A. Sabnis, and A.M. Edwards, *Polymyxin and lipopeptide antibiotics: membrane- targeting drugs of last resort.* Microbiology-Sgm, 2022. **168**(2).
20. Mohapatra, S.S., S.K. Dwibedy, and I. Padhy, *Polymyxins, the last-resort antibiotics: Mode of action, resistance emergence, and potential solutions.* Journal of Biosciences, 2021. **46**(3).
21. Khadka, N.K., C.M. Aryal, and J.J. Pan, *Lipopolysaccharide-Dependent Membrane Permeation and Lipid Clustering Caused by Cyclic Lipopeptide Colistin.* Acs Omega, 2018. **3**(12): p. 17828-17834.
22. Velkov, T., et al., *Structure--activity relationships of polymyxin antibiotics.* J Med Chem, 2010. **53**(5): p. 1898-916.
23. Sabnis, A., et al., *Colistin kills bacteria by targeting lipopolysaccharide in the cytoplasmic membrane.* Elife, 2021. **10**.
24. Raetz, C.R. and C. Whitfield, *Lipopolysaccharide endotoxins.* Annu Rev Biochem, 2002. **71**: p. 635-700.
25. Bertani, B. and N. Ruiz, *Function and Biogenesis of Lipopolysaccharides.* EcoSal Plus, 2018. **8**(1).
26. Fahy, E., et al., *A comprehensive classification system for lipids.* J Lipid Res, 2005. **46**(5): p. 839-61.
27. Simpson, B.W. and M.S. Trent, *Pushing the envelope: LPS modifications and their consequences.* Nature Reviews Microbiology, 2019. **17**(7): p. 403-416.
28. Raetz, C.R., et al., *Lipid A modification systems in gram-negative bacteria.* Annu Rev Biochem, 2007. **76**: p. 295-329.
29. Dowhan, W., *The Raetz pathway for lipid A biosynthesis: Christian Rudolf Hubert Raetz, MD PhD, 1946-2011.* J Lipid Res, 2011. **52**(11): p. 1857-1860.
30. Raetz, C.R., *Biochemistry of endotoxins.* Annu Rev Biochem, 1990. **59**: p. 129-70.
31. Zahringer, U., B. Lindner, and E.T. Rietschel, *Molecular structure of lipid A, the endotoxic center of bacterial lipopolysaccharides.* Adv Carbohydr Chem Biochem, 1994. **50**: p. 211-76.
32. Hittle, L.E., et al., *Site-specific activity of the acyltransferases HtrB1 and HtrB2 in Pseudomonas aeruginosa lipid A biosynthesis.* Pathog Dis, 2015. **73**(8): p. ftv053.
33. Hofstaedter, C.E., et al., *Divergent Pseudomonas aeruginosa LpxO enzymes perform site-specific lipid A 2-hydroxylation.* mBio, 2024. **15**(2): p. e0282323.
34. Brozek, K.A. and C.R. Raetz, *Biosynthesis of lipid A in Escherichia coli. Acyl carrier protein-dependent incorporation of laurate and myristate.* J Biol Chem, 1990. **265**(26): p. 15410-7.
35. Gibbons, H.S., et al., *Oxygen requirement for the biosynthesis of the S-2-hydroxymyristate moiety in Salmonella typhimurium lipid A. Function of LpxO, A new Fe2+/alpha-ketoglutarate-dependent dioxygenase homologue.* J Biol Chem, 2000. **275**(42): p. 32940-9.
36. MacArthur, I., et al., *Role of pagL and lpxO in Bordetella bronchiseptica lipid A biosynthesis.* J Bacteriol, 2011. **193**(18): p. 4726-35.
37. Ernst, R.K., et al., *The Pseudomonas aeruginosa lipid A deacylase: selection for expression and loss within the cystic fibrosis airway.* J Bacteriol, 2006. **188**(1): p. 191-201.
38. King, J.D., et al., *Review: Lipopolysaccharide biosynthesis in Pseudomonas aeruginosa.* Innate Immunity, 2009. **15**(5): p. 261-312.
39. Chen, H.D. and E.A. Groisman, *The biology of the PmrA/PmrB two-component system: the major regulator of lipopolysaccharide modifications.* Annu Rev Microbiol, 2013. **67**: p. 83-112.
40. Groisman, E.A., *The pleiotropic two-component regulatory system PhoP-PhoQ.* Journal of Bacteriology, 2001. **183**(6): p. 1835-1842.
41. Ernst, R.K., et al., *The Pseudomonas seruginosa lipid A deacylase:: Selection for expression and loss within the cystic fibrosis airway.* Journal of Bacteriology, 2006. **188**(1): p. 191-201.
42. Guo, L., et al., *Lipid A acylation and bacterial resistance against vertebrate antimicrobial peptides.* Cell, 1998. **95**(2): p. 189-98.
43. Trent, M.S., et al., *An inner membrane enzyme in Salmonella and Escherichia coli that transfers 4-amino-4-deoxy-L-arabinose to lipid A: induction on polymyxin-resistant mutants and role of a novel lipid-linked donor.* J Biol Chem, 2001. **276**(46): p. 43122-31.
44. Lo Sciuto, A. and F. Imperi, *Aminoarabinosylation of Lipid A Is Critical for the Development of Colistin Resistance in.* Antimicrobial Agents and Chemotherapy, 2018. **62**(3).
45. Moskowitz, S.M., R.K. Ernst, and S.I. Miller, *PmrAB, a two-component regulatory system of Pseudomonas aeruginosa that modulates resistance to cationic antimicrobial peptides and addition of aminoarabinose to lipid A.* Journal of Bacteriology, 2004. **186**(2): p. 575-579.
46. Olaitan, A.O., S. Morand, and J.M. Rolain, *Mechanisms of polymyxin resistance: acquired and intrinsic resistance in bacteria.* Front Microbiol, 2014. **5**: p. 643.
47. Hsieh, Y.P., et al., *Widespread fungal-bacterial competition for magnesium lowers bacterial susceptibility to polymyxin antibiotics.* PLoS Biol, 2024. **22**(6): p. e3002694.
48. Macfarlane, E.L., et al., *PhoP-PhoQ homologues in Pseudomonas aeruginosa regulate expression of the outer-membrane protein OprH and polymyxin B resistance.* Mol Microbiol, 1999. **34**(2): p. 305-16.
49. Yang, H., et al., *Lipid A Structural Determination from a Single Colony.* Anal Chem, 2022. **94**(21): p. 7460-7465.
50. Lee, J.Y., et al., *Evolved resistance to colistin and its loss due to genetic reversion in Pseudomonas aeruginosa.* Sci Rep, 2016. **6**: p. 25543.
51. Jeannot, K., et al., *Detection of Colistin Resistance in Pseudomonas aeruginosa Using the MALDIxin Test on the Routine MALDI Biotyper Sirius Mass Spectrometer.* Front Microbiol, 2021. **12**: p. 725383.
52. Lo Sciuto, A., et al., *Genetic Basis and Physiological Effects of Lipid A Hydroxylation in Pseudomonas aeruginosa PAO1.* Pathogens, 2019. **8**(4).
53. de Kievit, T.R., et al., *Molecular cloning and characterization of the rfc gene of Pseudomonas aeruginosa (serotype O5).* Mol Microbiol, 1995. **16**(3): p. 565-74.
54. Kaluzny, K., P.D. Abeyrathne, and J.S. Lam, *Coexistence of two distinct versions of O-antigen polymerase, Wzy-alpha and Wzy-beta, in Pseudomonas aeruginosa serogroup O2 and their contributions to cell surface diversity.* J Bacteriol, 2007. **189**(11): p. 4141-52.
55. Ting, S.Y., et al., *Discovery of coordinately regulated pathways that provide innate protection against interbacterial antagonism.* Elife, 2022. **11**.
56. Rainey, P.B. and M. Travisano, *Adaptive radiation in a heterogeneous environment.* Nature, 1998. **394**(6688): p. 69-72.
57. Santos-Lopez, A., et al., *Evolutionary pathways to antibiotic resistance are dependent upon environmental structure and bacterial lifestyle.* Elife, 2019. **8**.
58. Habets, M.G., et al., *The effect of population structure on the adaptive radiation of microbial populations evolving in spatially structured environments.* Ecol Lett, 2006. **9**(9): p. 1041-8.
59. Lin, J., et al., *Resistance and Heteroresistance to Colistin in Pseudomonas aeruginosa Isolates from Wenzhou, China.* Antimicrobial Agents and Chemotherapy, 2019. **63**(10).

60. Moskowitz, S.M., et al., *PmrB mutations promote polymyxin resistance of Pseudomonas aeruginosa isolated from colistin-treated cystic fibrosis patients.* Antimicrob Agents Chemother, 2012. **56**(2): p. 1019-30.
61. Jochumsen, N., et al., *The evolution of antimicrobial peptide resistance in Pseudomonas aeruginosa is shaped by strong epistatic interactions.* Nature Communications, 2016. **7**.
62. Dosselmann, B., et al., *Rapid and Consistent Evolution of Colistin Resistance in Extensively Drug-Resistant Pseudomonas aeruginosa during Morbidostat Culture.* Antimicrob Agents Chemother, 2017. **61**(9).
63. Hofstaedter, C.E., et al., *Pseudomonas aeruginosa Lipid A Structural Variants Induce Altered Immune Responses.* Am J Respir Cell Mol Biol, 2024. **71**(2): p. 207-218.
64. Bereswill, S., H. Mulcahy, and S. Lewenza, *Magnesium Limitation Is an Environmental Trigger of the Pseudomonas aeruginosa Biofilm Lifestyle.* PLoS ONE, 2011. **6**(8).
65. Torres, D.A., et al., *Colistin resistance in Gram-negative bacteria analysed by five phenotypic assays and inference of the underlying genomic mechanisms.* BMC Microbiol, 2021. **21**(1): p. 321.
66. Mondal, A.H., et al., *A Review on Colistin Resistance: An Antibiotic of Last Resort.* Microorganisms, 2024. **12**(4).
67. Trebosc, V., et al., *Dissecting Colistin Resistance Mechanisms in Extensively Drug-Resistant Acinetobacter baumannii Clinical Isolates.* mBio, 2019. **10**(4).
68. Xu, T., et al., *Magnesium Links Starvation-Mediated Antibiotic Persistence to ATP.* mSphere, 2020. **5**(1).
69. Hmelo, L.R., et al., *Precision-engineering the Pseudomonas aeruginosa genome with two-step allelic exchange.* Nat Protoc, 2015. **10**(11): p. 1820-41.
70. Yang, H., et al., *A Multimodal System for Lipid A Structural Analysis from a Single Colony.* Anal Chem, 2024. **96**(34): p. 13838-45.
71. Helander, I.M. and T. Mattila-Sandholm, *Fluorometric assessment of gram-negative bacterial permeabilization.* J Appl Microbiol, 2000. **88**(2): p. 213-9.

Acknowledgments

We thank the Ernst, Dandekar, and Malik lab members for valuable discussions and their comments on the manuscript. We thank Nina Salama for her suggestion to look for specific lipid A modifications and Steve MacFariane and the Fred Hutch Electron Microscopy & CryoEM Core for supporting scanning electron microscopy experiments. The following funding agencies funded this study: Cystic Fibrosis Foundation HSIEH24F0 and HSIEH21F0-CI (to YPH), Cystic Fibrosis Foundation ERNST23G0 and NIH AI104895 (to RKE), NIH R35 GM152107 (to AAD), and Howard Hughes Medical Institute Investigator award (to HSM). Funding agencies played no role in the study design or publication decision.

Author contributions

Conceptualization: YPH, IPO, RKE, AAD, HSM
Methodology: YPH, IPO
Investigation: YPH, WS, ZW, IPO, HY, LMV
Visualization: YPH, IPO, WS, AAD, HSM
Funding acquisition: YPH, RKE, AAD, HSM
Supervision: YPH, RKE, AAD, HSM
Writing-original draft: YPH, IPO, AAD, HSM
Writing-review & editing: WS, ZW, HY, LMV, RKE

Competing interest statement

The authors declare they have no competing interests.

Materials and Methods

Fungal and bacterial strains used in this study

All bacterial and fungal strains used in this study are listed in Table S2. Bacterial strains in this study were derived from *P. aeruginosa* PAO1. Yeast strains were derived from *C. albicans* SC5314. Unless otherwise specified, all experiments were performed in Brain Heart Infusion Broth (BHI, Sigma-Aldrich), buffered with 10% MOPS and 2% glucose to pH 7.0, followed by filter sterilization. All strains were grown at 30°C or 37°C. For antibiotics used in this study, 100 μg/mL gentamicin was used to select against Gram-negative bacteria. 50 μg/mL nystatin was used to select against *C. albicans*. Colistin (Sigma-Aldrich) was prepared as a 10 mg/mL stock solution.

Cell Lines

HEK-293T/17 and HeLa cells were grown on treated tissue-culture plates in DMEM (Thermo Fisher #11965118) containing high-glucose and L-glutamine with 1x penicillin/streptomycin (Thermo Fisher #15140122) and 10% fetal bovine serum (Gibco #10437028). Cells were grown at 37°C, 5% CO_2 in humidified incubators, and passaged by digestion with 0.05% trypsin-EDTA (Thermo Fisher #25300120).

Co-culture colistin survival assay

All experiments began with bacterial or fungal cultures that were grown overnight. The starter cultures were diluted either 1:100 (for bacterial cultures) or 1:50 (for fungal cultures) in BHI and cultured for ~4-5 hours to reach the log phase. Refreshed bacterial and fungal strains were added to BHI to reach the final bacterial cell density at 2.5 x 10^4 cells/mL and fungal cell density at 5 x 10^5 cells/mL for co-culture experiments. The identical amounts of bacterial or fungal cells were added separately in fresh BHI media as monoculture controls. These cultures were incubated for 18 hours at 37°C with shaking. To equalize bacterial cell numbers in these two conditions before colistin treatment, the cell density of monoculture samples was adjusted to optical density at 600 nm (OD_{600}) 0.3 to match the bacterial cell density after 18 hours of growth in co-culture. Both equilibrated monoculture and co-culture samples were split into two 1 mL culture tubes. 192 μg/ml of colistin was added to one of the tubes. Cells in both tubes were incubated at 37°C for 1.5 hours, and the bacterial viability was determined by enumerating colony-forming units (CFU) in each condition. Bacterial survival was calculated as the ratio of CFU upon colistin treatment relative to no colistin (average of four replicates from two technical replicates).

Antibiotic MIC assays

MICs were determined using a standard serial broth dilution method. Bacterial cells were cultured in BHI media overnight at 37°C with shaking. The overnight culture was diluted 1:100 into 2 mL of either BHI media or *C. albicans*-spent media for 5 hours. Eight serial dilutions of colistin (from 0 to 192 μg/mL or from 192 to 768 μg/mL) were prepared in the corresponding media in 96-well microtiter plates. Next, 3 μL of the log-phase culture was inoculated to each well with 200 μL media and titrated antibiotics. The plate was incubated at 37°C for 24 h, after which OD_{600} was measured using a microplate reader. The MIC of each strain was determined as the lowest concentration of antibiotics at which OD_{600} was half of the maximum OD_{600} observed in the absence of colistin. Three technical replicates were used to measure the MIC of each strain.

Mutation reconstruction in WT PAO1

For generating gene deletions in *P. aeruginosa*, an allelic exchange method was used [69]. Briefly, deletion constructs were incorporated into the pEXG2 plasmid and transformed into *E. coli* S17. The S17 donor was subsequently mixed with *P. aeruginosa* recipients on an LB agar plate at a 5:1 ratio of donor to recipient cells, and the cell mixture was incubated at 30°C overnight. The cell mixture was plated on LB agar plates with 100 μg/mL gentamicin to select for

cells containing the deletion plasmid integrated into the *P. aeruginosa* genome. Counterselection was performed with LB agar plates containing sucrose. Gene deletions were confirmed by Sanger sequencing of PCR products (GeneWiz, Azenta). Primers and Plasmids used for strain constructions are listed in Table S3.

Whole genome sequencing of evolutionary intermediates of evolved populations

Populations were sequenced at two-week intervals and at the endpoint by reviving each population from a freezer stock in the growth condition under which they evolved and grown for 24 h. For co-culture evolved populations, we treated them with nystatin to remove fungal cells, and a 3 ml bacterial culture was collected for DNA extraction using the DNeasy Blood & Tissue kit (Qiagen). Sequencing libraries were made and commercially sequenced by Illumina sequencers in SeqCenter (https://www.seqcenter.com/). Variant calling was done using the breseq software v0.37.1, and the *P. aeruginosa* PAO1 genome (GCF_00006765.1) was used as the reference genome. The average sequencing depth for populations was 222.5 fold (+/− 32.7), and the average genome coverage was 98.8 fold (+/− 0.04). Variants at >95% in each population were filtered for mutation calling. Mutations were manually curated by identifying unique variants in each evolved population compared to the ancestor.

Mass Spectrometry analysis of lipid A

Lipid A structural analysis was performed using Fast Lipid Analysis Technique (FLAT), as previously described [70]. Bacterial cultures were grown to the mid-log phase and pelleted. The pellet was scraped directly onto a steel MALDI target plate in duplicate with a pipette tip. FLAT extraction buffer (1 μL; 0.2 M anhydrous citric acid, 0.1 M trisodium citrate dihydrate, pH 4.5) was pipetted over bacterial spots. The FLAT target plate was incubated at 100°C in a humidified heat block for 30 minutes. Bacterial spots were washed with endotoxin-free water Gibco (Grand Island, NY, USA) and air-dried, followed by the addition of norharmane matrix (10mg/mL in 1:2 MeOH : CHCl3 – Sigma Aldrich, St. Louis, MO, USA). Mass spectra were collected in negative-ion mode using a Bruker timsTOF Flex. Agilent ESI Tune Mix was used as an external calibrant. Mass spectra were processed using DataAnalysis v3.4 software. Ions for tandem mass spectrometry were identified in DataAnalysis and fragmented in the gas phase between 70 and 90 eV. Each MS analysis was performed with at least two independent biological replicates. Mass spectra were analyzed using mMass v5.5.0. Table S1 describes all the m/z values determined in our experiments.

Outer membrane permeability assay

We used a previously established NPN uptake assay [23, 71]. Bacterial cells were grown to log phase in BHI or *C. albicans*-spent BHI. Cells were diluted to an OD_{600} 0.5 in 1ml 5mM HEPES, pH 7.2. One hundred and fifty μl bacterial suspension was added to wells of a black microtiter plate with clear-bottomed wells. The fluorescent probe N-phenyl-1-naphthylamine (NPN, Sigma Aldrich) was added to a final concentration of 10 μM. Fluorescence was measured immediately in a Cytation 5 plate reader using an excitation wavelength of 535 nm and an emission wavelength of 405 nm. Fluorescence measurements were obtained every 1min for 15 mins, and the degree of outer membrane permeability, referred to as the NPN uptake score, was calculated using the following equation: *(Fluorescence of sample with NPN - Fluorescence of sample without NPN)/ (Fluorescence of HEPES buffer with NPN – Fluorescence of HPES buffer without NPN)*

Scanning electron microscopy experiments

1mL log-phase cells in BHI were collected and fixed with formaldehyde. Duplicates of 50 μL of each sample were applied in a pool on poly-l-lysine coated coverslips for 30 min, rinsed with 0.1M sodium cacodylate buffer, and treated with 1% osmium tetroxide for 1 hour. The coverslips were then rinsed with cacodylate buffer, dehydrated through a graded series of alcohols, infiltrated with HMDS (Electron Microscopy Sciences, Hatfield, PA), and allowed to air dry. Coverslips were mounted on stubs and sputter coated with gold/palladium (Denton Desk IV, Denton Vacuum, Moorestown, NJ). Samples were imaged on a JSM 6610 LV scanning electron microscope at 15kV and 12mm working distance (JEOL, Tokyo, Japan).

Competitive fitness assay

WT PAO1 with chromosomally integrated mCherry was used as the reference strain in fitness competition with deletion mutants, either in BHI media only or in BHI media in co-culture with *C. albicans*. All bacterial and yeast strains were incubated in BHI at 37°C to log phase. A non-fluorescent test strain was mixed with the fluorescence-labeled reference strain at a ratio of 1:1. Part of the cell mixture was used to determine the initial ratio of sample and reference strains using flow cytometry (BD FACSymphony A5 Cell Analyzer). Then, 10 μl of cell mixture was inoculated separately in 2 ml BHI alone (monoculture) or 2 ml BHI with 2×10^5 *C. albicans* cells (co-culture) and grown in BHI at 37°C for 18 h. After 18 h, monoculture samples were diluted 100-fold to measure the ratio of sample and reference strain. For co-culture samples, a low-speed spin (500xg for 8 min) was applied to separate bacterial and fungal populations. Supernatants enriched with bacterial cells were identified using flow cytometry. For each sample, at least 30,000 cells were collected and the FACS data were analyzed by the FlowJo 10.4.1 software. The reference strain was cultured separately to estimate the number of generations during the experiment. Each experiment was conducted in at least 2 biological and 2 technical replicates. To calculate the relative fitness, w, of each sample strain to the reference strain, we followed the formula: $w = 1+s$, where selection coefficient $s = [\ln(\text{sample/reference})t - \ln(\text{sample/reference})t{=}0]/t$, where t = number of generations and (sample/reference) is the ratio between a sample strain and the reference strain.

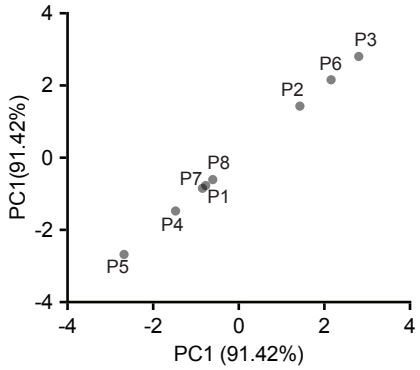

evolved population	P2	P3	P6	P1	P5	P7	P4	P8
% survival to colistin	32	9	20	68	100	69	81	66

Fig. S1. PCA analysis of bacterial survival to 192μg/ml colistin in co-culture. *P. aeruginosa* survival to 192μg/ml colistin in co-culture was measured using the colistin survival assay and reported in our previous study. PCA analysis and mean survival to colistin of all 8 replicate evolved populations are shown in the corresponding upper and lower panels. Populations P2, P3, and P6 are more sensitive to colistin than the rest of evolved populations.

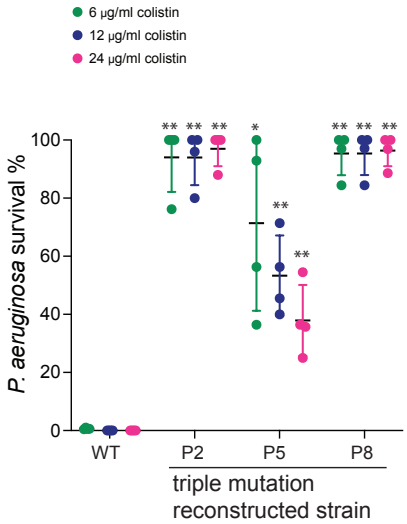

Fig. S2. Triple-mutation-reconstructed strain shows significantly increased survival to a range of low concentrations of colistin in co-culture. *P. aeruginosa* survival to low concentrations of colistin in co-culture was measured using the colistin survival assay. Survival of triple mutants to 6, 12, and 24 μg/ml colistin is shown in green, blue, and magenta, respectively. P2-derived triple mutant contains *htrB2*, *PA4824*, and the *oprH*/*phoPQ* promoter mutations. P5-derived triple mutant contains *htrB2*, *PA4824*, and *lpxO2* mutations. P8-derived triple mutant contains lpxA, PA4824, and the *oprH*/*phoPQ* promoter mutations. Mean ± std of 4 biological replicates is shown. The survival of WT PAO1 in three conditions is used as the reference for statistical analysis (**$p < 0.01$, *$p < 0.05$, Dunnett's one-way ANOVA test).

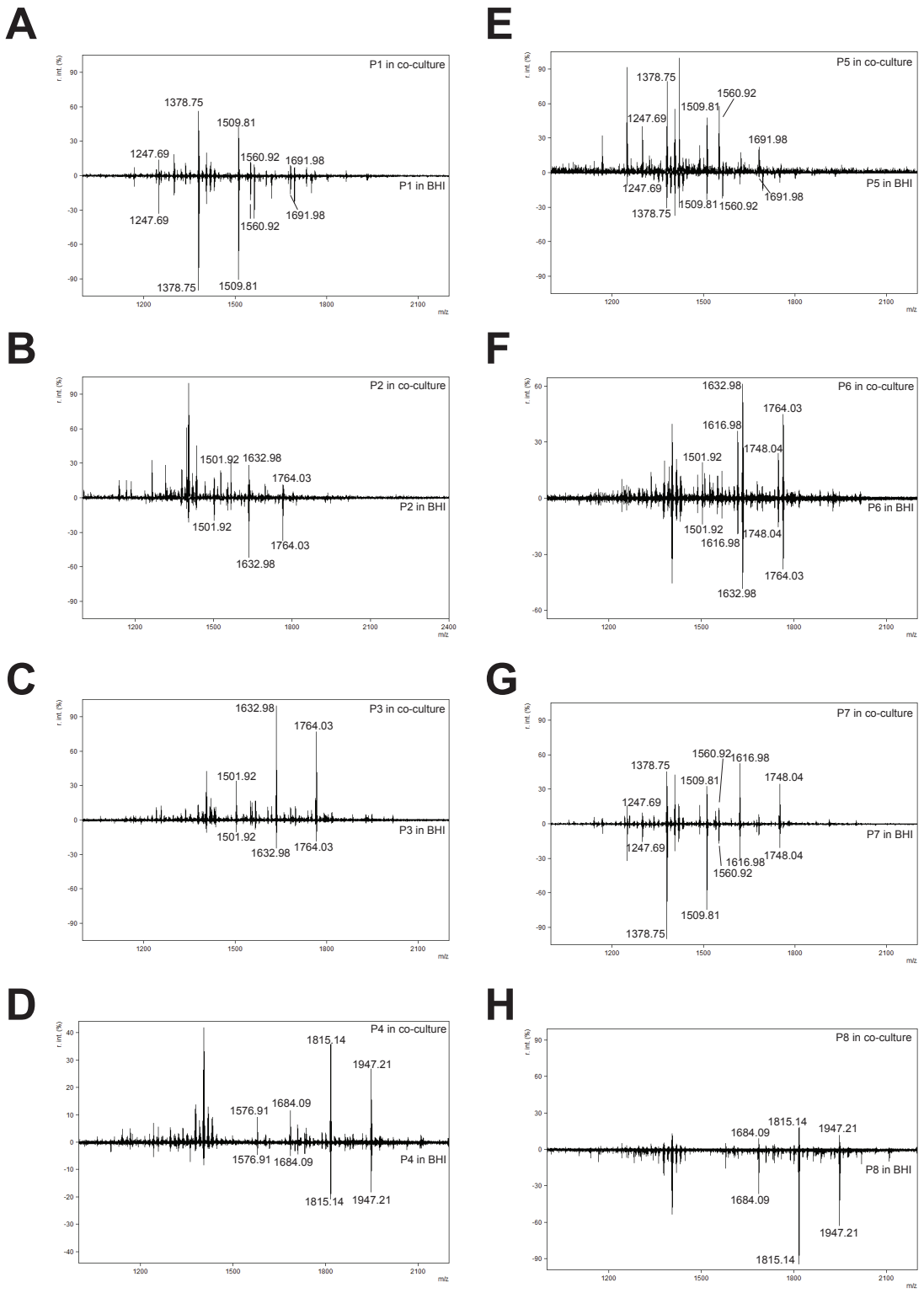

Fig. S3. All replicate populations exhibit similar MS spectra in monoculture and co-culture conditions. **(A-H)** Mass spectra of lipid A for P1 through P8 are shown cocultured with C. albicans (top) and alone (bottom). Variations in peak height are due to variations in total peak intensity between samples.

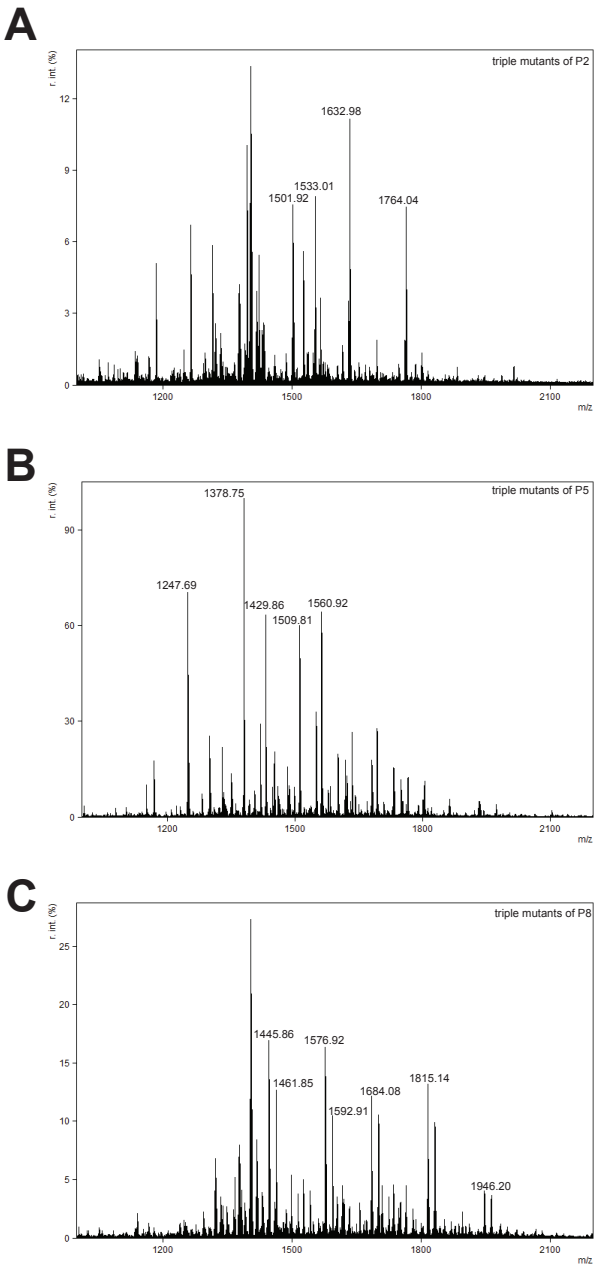

Fig. S4. MS spectra of triple-mutation-reconstructed strains are similar to those of endpoint populations. Mass spectra of lipid A from all triple mutants. **(A)** Lipid A MS of P2 triple reconstruction mutant. Peaks at m/z 1501.92, 1632.98, and 1764.04 were present in the original P2. The peak at 1533.01 was not present at a high intensity in the original P2. **(B)** Lipid A MS of the P5 triple mutant reconstruction. All peaks present were also present in the original P5. **(C)** Lipid A MS of P8 triple mutant reconstruction. Peaks at 1684.08, 1815.14, and 1946.20 were all present in the original P8. Peaks at 1445.86 and 1576.92 were not present in P8 and represent penta-acylated lipid A without PagP-mediated palmitoylation. All peaks that are +15.99 m/z from previously mentioned peaks contain LpxO1-mediated 2-hydroxylation, which is also not present in the original P8.

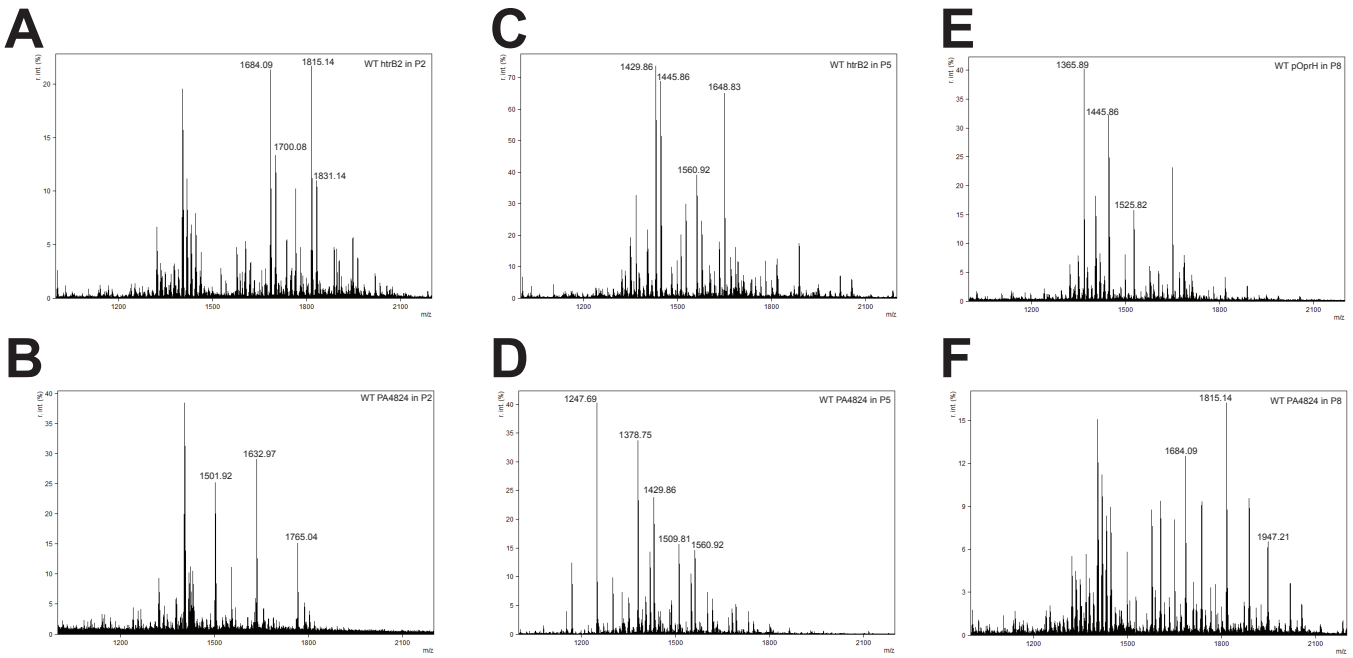

Fig. S5. MS spectra of single mutation reversion strains. Mass spectra of lipid A from all single mutation reversion strains**. (A)** MS of WT *htrB2* in P2. Peaks present indicate hexa-acylated lipid A with HtrB2 function restored. **(B)** MS of WT *PA4824* in P2. All peaks present were also found in the original P2. **(C)** MS of WT *htrB2* in P5. Peaks present indicate penta-acylated lipid A with restored function of *htrB2*. **(D)** MS of wild-type PA4824 in P5. All peaks present were also found in the original P5. **(E)** MS of WT *oprH/phoPQ* promoter in P8. Peaks present are penta-acylated lipid A varying in phosphorylation level, indicating a lack of PagP-mediated palmitoylation, as well as a lack of L-Ara4N addition. **(F)** MS of WT *PA4824* in P8. All peaks present were also found in the original P8.

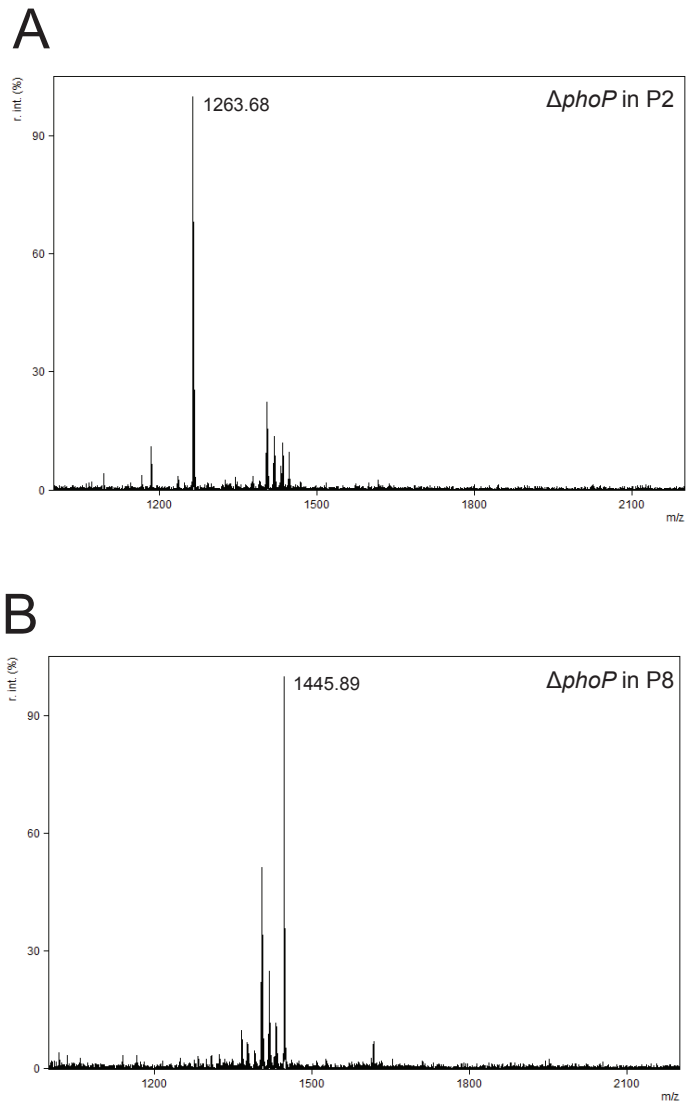

Fig. S6. MS spectra of ΔphoP in the endpoint strains of P2 and P8. Δ*phoP* in P2 **(A)** and P8 **(B)** show lipid A without aminoarabinose addition and PagP-mediated acylation. **(A)** FLAT followed by MALDI-TOF MS of Δ*phoP* in P2 yielded only one lipid A peak at 1263.68 *m/z*. This corresponds to a tetra-acylated lipid A structure lacking the previously present aminoarabinose additions and PagP-mediated palmytoylation in P2. **(B)** FLAT followed by MALDI-TOF MS of Δ*phoP* in P8 yielded only one major lipid A ion corresponding to the penta-acylated, singly hydroxylated 1445.89 *m/z*, lacking the aminoarabinose additions and PagP-mediated C16 addition that were present in the final P8 evolved clone.

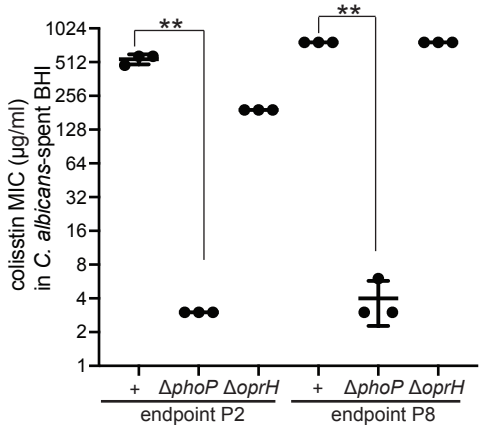

Fig. S7. Deletion of phoP, not oprH, in P2 and P8 clones reduced colistin resistance. Colistin resistance was measured by MIC in Mg^{2+}-depleted *C. albicans*-spent media. Mean ± std of 3 biological replicates is shown. (**$p < 0.01$, Mann Whitney U test)

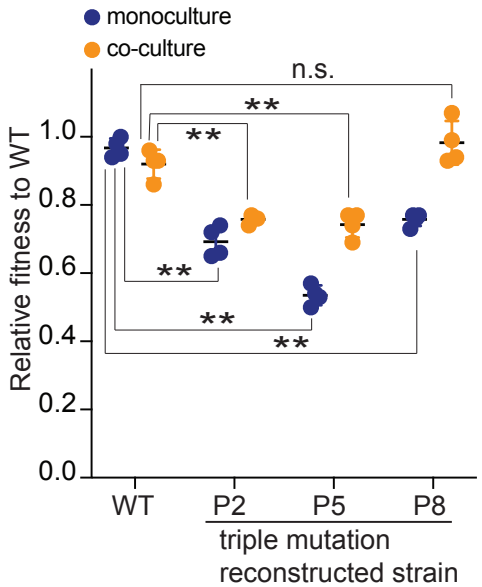

Fig. S8. Fitness costs of triple-mutation-reconstructed strains in monoculture and co-culture conditions. The relative fitness of P. aeruginosa strains to WT in conditions without colistin was measured by competitive fitness assay. Fitness in monoculture is shown in blue, and fitness in fungal co-culture is shown in orange. Triple-mutation-reconstructed strains derived from populations P2, P5, and P8 were used to quantify the fitness effects of early-occurring mutations. Mean ± std of 4 biological replicates is shown. (**$p < 0.01$, Dunnett's one-way ANOVA test)

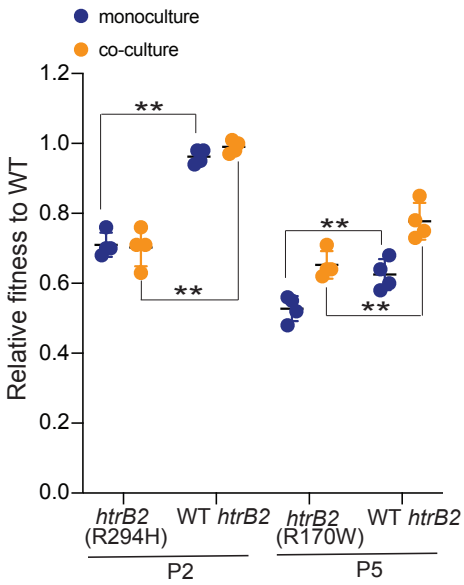

Fig. S9. htrB2 reversion increases the fitness of the population P2 and P5 in monoculture and co-culture conditions. The relative fitness of P. aeruginosa strains to WT in conditions without colistin was measured by competitive fitness assay. Fitness in monoculture is shown in blue, and fitness in fungal co-culture is shown in orange. Mean ± std of 4 biological replicates is shown. (**$p < 0.01$, *$p < 0.05$, one-tailed Mann Whitney test)

Table S1. Peak table of all major and minor lipid A species present in MS analysis Every m/z peak representative of lipid A structure found in FLAT followed by MALDI-TOF MS. C3' and C2' refer to the third and second carbons on the glucosamine on the left side, while C3 and C2 refer to the third and second carbons of the right glucosamine, respectively. Phosphorylation status and aminoarabinose status are not site-specific.

Calculated m/z	C-3'	C-2'	C-3	C-2	Phosphorylation	Aminoarabinose
1247.6953	C10(3-OH)	C12(3-OH)	H	C12(3-OH):C12	Diphosphate	None
1263.693	C10(3-OH)	C12(3-OH)	H	C12(3-OH):C12(2-OH)	Diphosphate	None
1365.8772	C10(3-OH)	C12(3-OH):C12	H	C12(3-OH):C12(2-OH)	Monophosphate	None
1378.7535	C10(3-OH)	C12(3-OH)	H	C12(3-OH):C12	Diphosphate	Single
1417.826	C10(3-OH)	C12(3-OH)	C10(3-OH)	C12(3-OH):C12	Diphosphate	None
1429.8623	C10(3-OH)	C12(3-OH):C12	H	C12(3-OH):C12	Diphosphate	None
1433.823	C10(3-OH)	C12(3-OH)	C10(3-OH)	C12(3-OH):C12(2-OH)	Diphosphate	None
1445.8572	C10(3-OH)	C12(3-OH):C12	H	C12(3-OH):C12(2-OH)	Diphosphate	None
1461.8522	C10(3-OH)	C12(3-OH):C12	H	C12(3-OH):C12(2-OH)	Diphosphate	None
1480.9292	C10(3-OH)	C12(3-OH):C12	H	C12(3-OH):C12	Monophosphate	Single
1485.9249	C10(3-OH):C16	C12(3-OH)	H	C12(3-OH):C12	Diphosphate	None
1496.9241	C10(3-OH)	C12(3-OH):C12	H	C12(3-OH):C12(2-OH)	Monophosphate	Single
1501.9199	C10(3-OH):C16	C12(3-OH)	H	C12(3-OH):C12(2-OH)	Diphosphate	None
1509.8188	C10(3-OH)	C12(3-OH)	H	C12(3-OH):C12	Diphosphate	Double
1548.8842	C10(3-OH)	C12(3-OH)	C10(3-OH)	C12(3-OH):C12	Diphosphate	Single
1560.9206	C10(3-OH)	C12(3-OH):C12	H	C12(3-OH):C12	Diphosphate	Single
1564.8812	C10(3-OH)	C12(3-OH)	C10(3-OH)	C12(3-OH):C12(2-OH)	Diphosphate	Single
1576.9155	C10(3-OH)	C12(3-OH):C12	H	C12(3-OH):C12(2-OH)	Diphosphate	Single
1592.9104	C10(3-OH)	C12(3-OH):C12(2-OH)	H	C12(3-OH):C12(2-OH)	Diphosphate	Single
1599.9954	C10(3-OH)	C12(3-OH):C12	C10(3-OH)	C12(3-OH):C12	Diphosphate	None
1615.9903	C10(3-OH)	C12(3-OH):C12	C10(3-OH)	C12(3-OH):C12(2-OH)	Diphosphate	None
1616.9832	C10(3-OH):C16	C12(3-OH)	H	C12(3-OH):C12	Diphosphate	Single
1631.9853	C10(3-OH)	C12(3-OH):C12(2-OH	C10(3-OH)	C12(3-OH):C12(2-OH)	Diphosphate	None
1632.9781	C10(3-OH):C16	C12(3-OH)	H	C12(3-OH):C12(2-OH)	Diphosphate	Single
1668.092	C10(3-OH):C16	C12(3-OH):C12	H	C12(3-OH):C12	Diphosphate	None
1679.9424	C10(3-OH)	C12(3-OH)	C10(3-OH)	C12(3-OH):C12	Diphosphate	Double
1684.0869	C10(3-OH):C16	C12(3-OH):C12	H	C12(3-OH):C12(2-OH)	Diphosphate	None
1691.9561	C10(3-OH)	C12(3-OH):C12	H	C12(3-OH):C12	Diphosphate	Double
1700.0818	C10(3-OH):C16	C12(3-OH):C12(2-OH)	H	C12(3-OH):C12(2-OH)	Diphosphate	None
1707.951	C10(3-OH)	C12(3-OH):C12	H	C12(3-OH):C12(2-OH)	Diphosphate	Double
1723.9687	C10(3-OH)	C12(3-OH):C12(2-OH)	H	C12(3-OH):C12(2-OH)	Diphosphate	Double
1748.0414	C10(3-OH):C16	C12(3-OH)	H	C12(3-OH):C12	Diphosphate	Double
1764.0363	C10(3-OH):C16	C12(3-OH)	H	C12(3-OH):C12(2-OH)	Diphosphate	Double
1799.1502	C10(3-OH):C16	C12(3-OH):C12	H	C12(3-OH):C12	Diphosphate	Single
1815.1452	C10(3-OH):C16	C12(3-OH):C12	H	C12(3-OH):C12(2-OH)	Diphosphate	Single

1831.1401	C10(3-OH):C16	C12(3-OH):C12(2-OH)	H	C12(3-OH):C12(2-OH)	Diphosphate	Single
1930.2085	C10(3-OH):C16	C12(3-OH):C12	H	C12(3-OH):C12	Diphosphate	Double
1946.1849	C10(3-OH):C16	C12(3-OH):C12	H	C12(3-OH):C12(2-OH)	Diphosphate	Double
1962.1983	C10(3-OH):C16	C12(3-OH):C12(2-OH)	H	C12(3-OH):C12(2-OH)	Diphosphate	Double

Table S2. Strains used in this study

Strain Name	Species	Genotype	Lab source	Additional Information
YPH-b1	*P. aeruginosa* PAO1	WT	PAO1 master strain from the Dandekar lab, UW	
YPH-b3	*P. aeruginosa* PAO1	WT mCherry (at neutral site)	Generated in this study	
YPH-b304	*P. aeruginosa* PAO1	*PA4824* (P224L) in PAO1	Generated in this study	Mutation reconstruction from P2
YPH-b370	*P. aeruginosa* PAO1	*htrB2* (R294H) in PAO1	Generated in this study	Mutation reconstruction from P2
YPH-b371	*P. aeruginosa* PAO1	P_{oprH} (A to G) in PAO1	Generated in this study	Mutation reconstruction from P2
YPH-b385	*P. aeruginosa* PAO1	*PA4824* (P224L) + P_{oprH} (A to G) in PAO1	Generated in this study	Mutation reconstruction from P2
YPH-b389	*P. aeruginosa* PAO1	*PA4824* (P224L) + *htrB2* (R294H) + P_{oprH} (A to G) triple mutation in PAO1	Generated in this study	Mutation reconstruction from P2
YPH-b365	*P. aeruginosa* PAO1	*htrB2* (R170W) in PAO1	Generated in this study	Mutation reconstruction from P5
YPH-b387	*P. aeruginosa* PAO1	*lpxO2* (D163A) in PAO1	Generated in this study	Mutation reconstruction from P5
YPH-b368	*P. aeruginosa* PAO1	*PA4824* (P224L) + *htrB2* (R170W) in PAO1	Generated in this study	Mutation reconstruction from P5
YPH-b418	*P. aeruginosa* PAO1	*PA4824* (P224L) + *lpxO2*(D163A) + *htrB2*(R170W) triple mutation in PAO1	Generated in this study	Mutation reconstruction from P5
YPH-b421	*P. aeruginosa* PAO1	P_{oprH} (A to C) in PAO1	Generated in this study	Mutation reconstruction from P8
YPH-b419	*P. aeruginosa* PAO1	P_{oprH} (A to C) + *lpxA* (G170C) in PAO1	Generated in this study	Mutation reconstruction from P8
YPH-b420	*P. aeruginosa* PAO1	*PA4824* (P224L) + P_{oprH} (A to C) + *lpxA* (G170C) triple mutation in PAO1	Generated in this study	Mutation reconstruction from P8
YPH-b429	*P. aeruginosa* PAO1	WT *htrB2* in P2	Generated in this study	
YPH-b451	*P. aeruginosa* PAO1	WT P_{oprH} in P2	Generated in this study	
YPH-b435	*P. aeruginosa* PAO1	WT *PA4824* in P2	Generated in this study	
YPH-b423	*P. aeruginosa* PAO1	WT *PA4824* in P5	Generated in this study	
YPH-b424	*P. aeruginosa* PAO1	WT *htrB2* in P5	Generated in this study	
YPH-b450	*P. aeruginosa* PAO1	WT *lpxO2* in P5	Generated in this study	
YPH-b426	*P. aeruginosa* PAO1	WT *PA4824* in P8	Generated in this study	
YPH-b425	*P. aeruginosa* PAO1	WT P_{oprH} in P8	Generated in this study	
YPH-b470	*P. aeruginosa* PAO1	*oprH* deletion in P2	Generated in this study	
YPH-b458	*P. aeruginosa* PAO1	*oprH* deletion in P8	Generated in this study	
YPH-b468	*P. aeruginosa* PAO1	*phoP* deletion in P2	Generated in this study	
YPH-b462	*P. aeruginosa* PAO1	*phoP* deletion in P8	Generated in this study	
YPH-b481	*P. aeruginosa* PAO1	*phoP* deletion + *pmrA* deletion in P2	Generated in this study	
YPH-b479	*P. aeruginosa* PAO1	*phoP* deletion + *pmrA* deletion in P5	Generated in this study	
YPH-b472	*P. aeruginosa* PAO1	*phoP* deletion + *pmrA* deletion in P8	Generated in this study	

YPH-b483	*P. aeruginosa* PAO1	*PA4824*(P224L) + *htrB2*(R294H) + P_{oprH} (A to G) triple mutation in PAO1 + *phoP* deletion	Generated in this study	Mutation reconstruction from P2
YPH-b476	*P. aeruginosa* PAO1	*PA4824*(P224L) + *lpxO2*(D163A) + *htrB2*(R170W) triple mutation in PAO1 + *phoP* deletion	Generated in this study	Mutation reconstruction from P5
YPH-b477	*P. aeruginosa* PAO1	*PA4824* (P224L) + P_{oprH} (A to C) + l*pxA* (G170C) triple mutation in PAO1 + *phoP* deletion	Generated in this study	Mutation reconstruction from P8
YPH-b485	*P. aeruginosa* PAO1	*PA4824*(P224L) + *htrB2*(R294H) + P_{oprH} (A to G) triple mutation in PAO1 + *phoP* deletion + *pmrA* deletion	Generated in this study	Mutation reconstruction from P2
YPH-b487	*P. aeruginosa* PAO1	*PA4824*(P224L) + *lpxO2*(D163A) + *htrB2*(R170W) triple mutation in PAO1 + *phoP* deletion + *pmrA* deletion	Generated in this study	Mutation reconstruction from P5
YPH-b486	*P. aeruginosa* PAO1	*PA4824*(P224L) + P_{oprH} (A to C) + *lpxA* (G170C) triple mutation in PAO1 + *phoP* deletion + *pmrA* deletion	Generated in this study	Mutation reconstruction from P8
YPH-y1	*C. albicans*	WT prototroph (SC5314)	From Dr. Alistair Brown	

Table S3. Primers used in this study

Primer number	Primer name	Primer sequence	Note
YPH_o1	pEXG2_linear_R_v3	GCTTGCTTTACATTTATGCTTCC	Gibson Assembly for making pEXG2-based deletion plasmid
YPH_o2	pEXG2_linear_F_v3	ACTCTAGAGGATCCCCGG	Gibson Assembly for making pEXG2-based deletion plasmid
YPH_401	Q5_PA4824_P224L_F	GCAGGCCGGActgCGGCTGCACC	for making point mutation using Q5 mutagenesis kit
YPH_402	Q5_PA4824_P224L_R	CAGCCGCTGTCGCCGGCC	for making point mutation using Q5 mutagenesis kit
YPH_403	PA4824_CDS_seq_F	GAGCTGAAGACACCGCTG	for sequencing *PA4824* P224L mutation
YPH_404	PA4824_3UTR_seq_R	AGGGAACGGGCTCATTGA	for sequencing *PA4824* P224L mutation
YPH_415	pEXG2-lpxO2-F	CACACATTATACGAGCCGGAAGCATAAATGTAAAGCAAGCG-CAGGCGCGTCCCTTC	Gibson Assembly for making pEXG2-based deletion plasmid
YPH_416	pEXG2-lpxO2-R	GGTACCGAATTCGAGCTCGAGCCCGGGGATCCTCTAGAG-TAACTGAAGGCCGAGGAGC	Gibson Assembly for making pEXG2-based deletion plasmid
YPH_419	pEXG2-htrB2-F	CACACATTATACGAGCCGGAAGCATAAATGTAAAGCAA-GCTCGCGGGCGCCC	Gibson Assembly for making pEXG2-based deletion plasmid
YPH_420	pEXG2-htrB2-R	GGTACCGAATTCGAGCTCGAGCCCGGGGATCCTCTAGAG-TCGGCGCTGGCGCA	Gibson Assembly for making pEXG2-based deletion plasmid
YPH_421	pEXG2-poprH-F	CACACATTATACGAGCCGGAAGCATAAATGTAAAGCAAGCGAA-GCGGATCGCGGC	Gibson Assembly for making pEXG2-based deletion plasmid
YPH_422	pEXG2-poprH-R	GGTACCGAATTCGAGCTCGAGCCCGGGGATCCTCTAGAG-TGCGGGGTCATTTAGAACTTG	Gibson Assembly for making pEXG2-based deletion plasmid
YPH_429	Q5_htrB2_R170W_F	TGGCCGCGAGtggCACAACCTCG	for making point mutation using Q5 mutagenesis kit
YPH_430	Q5_htrB2_R170W_R	CGGCGCTGGACGTAGTCGAAC	for making point mutation using Q5 mutagenesis kit
YPH_431	Q5_htrB2_R294H_F	GGCGCACCGGcatTTCAAGACCC	for making point mutation using Q5 mutagenesis kit
YPH_432	Q5_htrB2_R294H_R	CACAGGTACTGCTCGGGC	for making point mutation using Q5 mutagenesis kit
YPH_438	lpxO2_CDS_F	GCTTCTACCTGACCTGGT	for sequencing *lpxO2* mutation
YPH_439	lpxO2_CDS_R	GGCGGAGGATTCGGTAG	for sequencing *lpxO2* mutation
YPH_442	htrB2_CDS_F	CATTTCACCACCCTGGAG	for sequencing *htrB2* mutation
YPH_443	htrB2_CDS_R	CCCGGAAAGGATCAGGC	for sequencing *htrB2* mutation
YPH_456	newQ5_lpxO2_D163A_F	CCGCACCGCGgcccCTTCGGCGGC	for making point mutation using Q5 mutagenesis kit
YPH_457	newQ5_lpxO2_D163A_R	ATTCAGGTGGCTGCCGCC	for making point mutation using Q5 mutagenesis kit
YPH_460	Q5_pOprH_G_F	GCAAGCGTTCcggGGCGGTTCAG	for making point mutation using Q5 mutagenesis kit
YPH_461	Q5_pOprH_G_R	TGAACCCGGGCTGAA	for making point mutation using Q5 mutagenesis kit
YPH_476	pOprH-F	CAGTAGCTGGTACATCCAGA	for sequencing P_{oprH} mutation
YPH_477	pOprH-R	TCTTGCTCAGCTCCTGCA	for sequencing P_{oprH} mutation

YPH_478	pEXG2-phoP-F	ATTCCACACATTATACGAGCCGGAAGCATAAATGTAAAGCAA-GCCACCTGGGGCATCCGC	Gibson Assembly for making pEXG2-based deletion plasmid
YPH_479	pEXG2-phoP-R	TAAGGTACCGAATTCGAGCTCGAGCCCGGGGATCCTCTAGAG-TCAGGTAGAGCTGCTCGC	Gibson Assembly for making pEXG2-based deletion plasmid
YPH_480	phoP-DOWN_F	CCGGCCGCATCTCATCCGGAGGAACCTCTCCGTTCCCTGCG-CATC	Gibson Assembly for making pEXG2-based deletion plasmid
YPH_481	phoP-UP-R	ATCAGACGGATGCGCAGGGAACGGAGAGGTTCCTCCG-GATGAGAT	Gibson Assembly for making pEXG2-based deletion plasmid
YPH_496	phoP_check_F	TGCAGGCCGGTATCCT	for checking *phoP* deletion
YPH_497	phoP_check_R	CTGGTCGTAGATATAGCCGAG	for checking *phoP* deletion
YPH_498	pOprH_C_F	CCCGGGTTCCGCAAGCGTTCAGGGGCGG	for making point mutation using Q5 mutagenesis kit
YPH_499	pOprH_C_R	CTTGCGGAACCCGGGCTGAACGACTCG	for making point mutation using Q5 mutagenesis kit